Article

Neuron

Thalamic Spindles Promote Memory Formation during Sleep through Triple Phase-Locking of Cortical, Thalamic, and Hippocampal Rhythms

Highlights

- Spindles in-phase with slow oscillation up-states boost hippocampus-dependent memory
- Phase coupling of slow oscillations, spindles, and ripples underlies memory formation
- Thalamic spindle stimulation drives cross-regional co-occurrence of spindles
- Thalamic inhibition phase-locked to slow oscillation up-states impairs memory

Authors

Charles-Francois V. Latchoumane, Hong-Viet V. Ngo, Jan Born, Hee-Sup Shin

Correspondence

jan.born@uni-tuebingen.de (J.B.), shin@ibs.re.kr (H.-S.S.)

In Brief

Latchoumane et al. demonstrate a causal role of sleep spindles in memory formation. They show that optogenetic induction of thalamic spindles, when phase-locked to the slow oscillation up-state, enhances the triple coupling of slow oscillations-spindles-ripples together with hippocampus-dependent memory consolidation.

Latchoumane et al., 2017, Neuron *95*, 1–12
July 19, 2017
http://dx.doi.org/10.1016/j.neuron.2017.06.025

CellPress

Please cite this article in press as: Latchoumane et al., Thalamic Spindles Promote Memory Formation during Sleep through Triple Phase-Locking of Cortical, Thalamic, and Hippocampal Rhythms, Neuron (2017), http://dx.doi.org/10.1016/j.neuron.2017.06.025

Neuron
Article

Thalamic Spindles Promote Memory Formation during Sleep through Triple Phase-Locking of Cortical, Thalamic, and Hippocampal Rhythms

Charles-Francois V. Latchoumane,[1,2,6] Hong-Viet V. Ngo,[3,4,6] Jan Born,[3,5,*] and Hee-Sup Shin[1,2,7,*]
[1]Center for Cognition and Sociality, Institute for Basic Science, Yuseong-gu, 34141 Daejeon, Republic of Korea
[2]IBS school, University of Science and Technology, 34113 Daejeon, Republic of Korea
[3]Institute for Medical Psychology and Behavioral Neurobiology, University of Tuebingen, 72076 Tuebingen, Germany
[4]School of Psychology, University of Birmingham, B15 2TT Birmingham, UK
[5]Center for Integrative Neuroscience, University of Tübingen, 72076 Tuebingen, Germany
[6]These authors contributed equally
[7]Lead Contact
*Correspondence: jan.born@uni-tuebingen.de (J.B.), shin@ibs.re.kr (H.-S.S.)
http://dx.doi.org/10.1016/j.neuron.2017.06.025

SUMMARY

While the interaction of the cardinal rhythms of non-rapid-eye-movement (NREM) sleep—the thalamo-cortical spindles, hippocampal ripples, and the cortical slow oscillations—is thought to be critical for memory consolidation during sleep, the role spindles play in this interaction is elusive. Combining optogenetics with a closed-loop stimulation approach in mice, we show here that only thalamic spindles induced in-phase with cortical slow oscillation up-states, but not out-of-phase-induced spindles, improve consolidation of hippocampus-dependent memory during sleep. Whereas optogenetically stimulated spindles were as efficient as spontaneous spindles in nesting hippocampal ripples within their excitable troughs, stimulation in-phase with the slow oscillation up-state increased spindle co-occurrence and frontal spindle-ripple co-occurrence, eventually resulting in increased triple coupling of slow oscillation-spindle-ripple events. In-phase optogenetic suppression of thalamic spindles impaired hippocampus-dependent memory. Our results suggest a causal role for thalamic sleep spindles in hippocampus-dependent memory consolidation, conveyed through triple coupling of slow oscillations, spindles, and ripples.

INTRODUCTION

Sleep is known to support the consolidation of memory (Rasch and Born, 2013). The <1 Hz cortical slow oscillation (Steriade et al., 1993), thalamo-cortical spindles (Steriade et al., 1986) (7–15 Hz), and hippocampal sharp wave-ripples (Buzsáki et al., 1992) (100–250 Hz) represent the cardinal rhythms of non-rapid-eye-movement (NREM) sleep, and all these rhythms have been implicated in the consolidation of declarative (i.e., hippocampus-dependent) memory during sleep (Fogel and Smith, 2011; Friedrich et al., 2015; Logothetis et al., 2012; Marshall et al., 2006; Ngo et al., 2013; Schreiner et al., 2015; Wang et al., 2015). Importantly, it has been proposed that consolidation of hippocampus-dependent memory during NREM sleep essentially relies on the hierarchical nesting of these rhythms (Diekelmann and Born, 2010; Dudai et al., 2015; Phillips et al., 2012). Phase-locking occurs such that ripples accompanying neural memory reactivation in the hippocampus nest into the excitable troughs of the spindle oscillation, which themselves nest into the excitable up-state of the slow oscillation (Clemens et al., 2007; Siapas and Wilson, 1998; Sirota et al., 2003; Staresina et al., 2015). This phase-locking presumably favors the redistribution of the representation from predominantly hippocampal toward neocortical networks that serve as long-term storage sites (Diekelmann and Born, 2010; Dudai et al., 2015).

Several studies have demonstrated a causal relationship between increased slow oscillation and memory consolidation in humans (Marshall et al., 2006; Ngo et al., 2013). Using timed electrical stimulation in rats, Maingret et al. (2016) provided evidence that reinforcing the endogenous temporal coordination between hippocampal sharp wave-ripples, cortical slow waves, and spindles can enhance the consolidation of hippocampus-dependent spatial memory. However, so far, there is no experimental evidence demonstrating a causal influence specifically of thalamic activity on the phase-locking between cortical slow oscillations and the subordinate rhythms—thalamo-cortical spindles and hippocampal ripples—in the process of memory formation. This is even more surprising as thalamic spindles emerging first during ontogeny (Khazipov et al., 2004), as well as in the course of human nocturnal sleep (Aeschbach and Borbély, 1993; Clemens et al., 2007), are suspected to play a central role in forming memory during sleep.

Using closed-loop, optogenetic stimulation of the thalamic reticular nucleus (TRN) to induce spindle activity in mice (Figure 1A), we show that only spindles induced during the slow oscillation up-state—that is in-phase coupling—enhance memory for previously learned hippocampus-dependent tasks, whereas spindles occurring out-of-phase with the slow

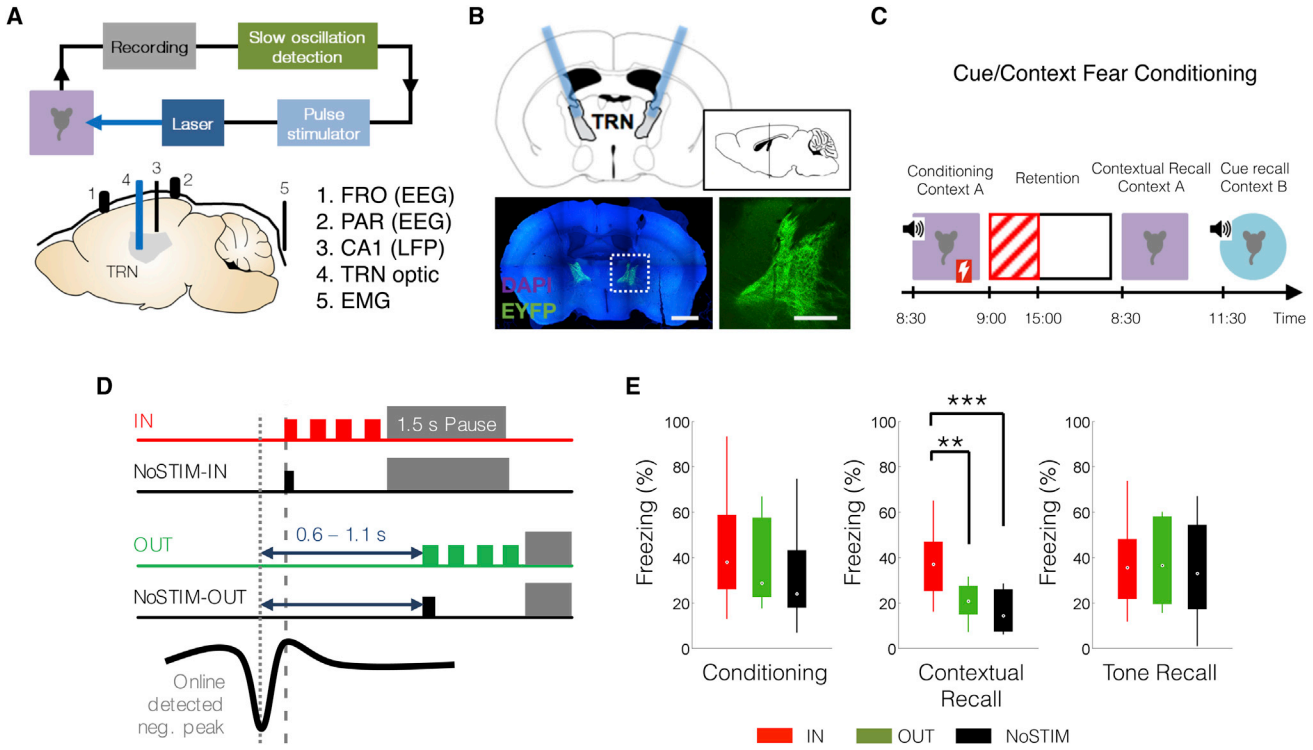

Figure 1. Spindle Stimulation of trn Parvalbumin Neurons In-Phase with Slow Oscillation Up-States Enhances Hippocampal-Dependent Memory

(A) Schema of EEG/LFP recordings and setup for closed-loop optogenetic stimulation.

(B) Schematic depiction of coronal and sagittal (top) positioning of optic fiber cannulas in the anterior ventral region of the TRN (bottom, left; scale bar, 1 mm) and the specifically high expression of mhChR2-EYFP in TRN (bottom, right; scale bar, 100 μm) parvalbumin neurons.

(C) Mice were tested on a combined cued/contextual fear-conditioning task. Following a learning phase, the animals were allowed to sleep and were subjected to one of three stimulation protocols for 6 hr (red hatched area). Recall of memory started 24 hr after the learning phase.

(D) Schematic of the stimulation protocols: mice were optogenetically stimulated with four light pulses (8 Hz, 62.5 ms on/off) as soon as they entered NREM sleep, inducing a spindle-like signal (Kim et al., 2012). Stimulation was applied such that it occurred during a slow oscillation up-state (IN, in-phase, n = 8, red trace) or with a random delay between 0.5 and 1.0 s after a slow oscillation up-state (OUT, out-of-phase, n = 8, green trace) and was then followed by a 1.5 s pause. In the no-stimulation condition, no light pulses were presented, but the time points corresponding to the in-phase (NoSTIM-IN, n = 10, upper black trace) and out-of-phase (NoSTIM-OUT, n = 10, lower black trace) stimulations were marked like for the stimulation conditions.

(E) Freezing level in the last minute of conditioning (left), recall of fear context (middle; average of the first 4 min), and fear cue (right; freezing at the delivery of the tone expressed as percentage of time freezing) were measured during a recall test 24 hr after learning for the in-phase (red bars), out-of-phase (green bars), and no-stimulation condition (black bars). ***$p < 0.001$, **$p < 0.01$ for post hoc pairwise comparisons. Data are shown as box-whisker plots with box limits representing the first and third quartile and whiskers indicating the data range.

oscillation remain ineffective. Furthermore, in-phase spindle-like stimulation enhanced the co-occurrence of frontal cortical spindles and ripples and, consequently, triplets of slow oscillation-spindle-ripple events.

RESULTS

Spindle-like Stimulation In-Phase with Slow Oscillation Up-States Enhances Memory

We tested transgenic mice expressing channelrhodopsin2 (ChR2) in parvalbumin (Prv)-expressing inhibitory neurons (Prv-mhChR2-EYFP; n = 26), a dominant subpopulation of the TRN that is sparse in surrounding thalamic nuclei (Asrican et al., 2013; Zhao et al., 2011) (Figure 1B; see also Figure S1), on a combined cued/contextual fear-conditioning (FC) task in which a 30 s tone followed by a 2 s shock was delivered in context A during conditioning (Boyce et al., 2016; Xu and Südhof, 2013) (see STAR Methods for details; Figure 1C). Retrieval was assessed 24 hr later by measuring freezing (1) to the same context A, as a readout of hippocampal contextual fear memory, and (2) to a tone delivered in a different context B, as a readout of cued fear memory that is not essentially dependent on the hippocampus. During the first 6 hr following conditioning, the mice were subjected to one of three stimulation protocols (Figure 1D; Figure S3; see also Method Details section). In-phase mice (IN) received spindle-like optogenetic stimulation (62.5 ms on/off, 4 pulses) to the TRN during NREM sleep, which occurred in synchrony with the up-states of online-detected slow oscillations. Out-of-phase mice (OUT) were likewise stimulated during NREM sleep but with a random delay between 0.5 and 1.0 s following identification of a slow oscillation up-state. Control mice received no stimulation (NoSTIM). At retrieval,

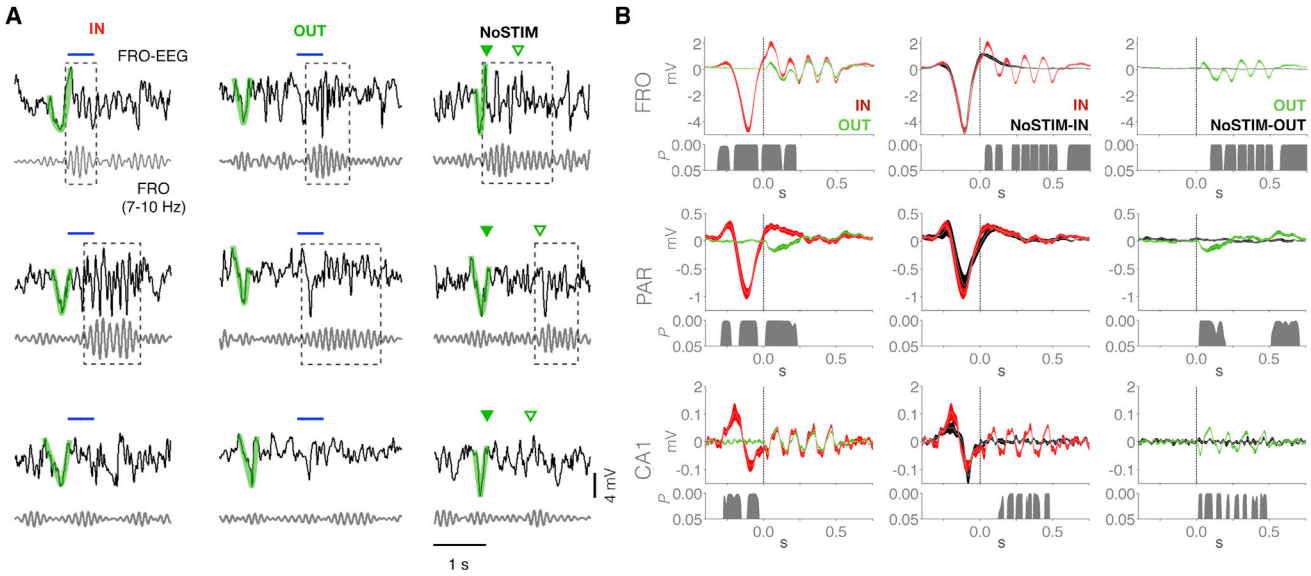

Figure 2. Effect of Thalamic Spindle Stimulation on Cortical EEG and Hippocampal LFP

(A) Three representative EEG traces from frontal (FRO) recording electrode for each of the three experimental protocols (3 s raw signals and signals filtered in the 7–10 Hz spindle band): in-phase, out-of-phase, and no-stimulation. The top two rows show examples with co-occurring spindle, whereas the bottom row shows cases with no identified spindle events. Online-detected slow oscillations that trigger the stimulation are highlighted in green. Intervals corresponding to light stimulation are indicated by blue bars; the starts of intervals for the no-stimulation condition corresponding to in-phase (NoSTIM-IN) and out-of-phase (NoSTIM-OUT) protocols are indicated by green filled and empty triangles, respectively. Offline-identified discrete spindle events are framed by dashed rectangles.

(B) Mean ± SEM. EEG signals (filtered at 0.3–30 Hz) over frontal (FRO, top) and parietal (PAR, middle) cortical areas and averaged LFP signals from the hippocampal CA1 (bottom), time-locked to stimulation onset, across all mice under in-phase (red lines), out-of-phase (green), and no-stimulation (black) conditions. Vertical dashed black lines indicate stimulation onset (t = 0). Left column: comparison of in-phase and out-of-phase stimulation. Middle and right columns: comparison of in-phase (middle) and out-of-phase (right) stimulation with corresponding periods in the no-stimulation control. Significant differences (p values) are indicated at the bottoms of panels. Please note that the SEM was generally smaller than 0.2 mV and is thus not discernable from the trace of the mean in some cases.

contextual fear memory was selectively enhanced in in-phase mice, whereas out-of-phase mice showed no improvement in contextual fear memory compared with no-stimulation controls (Figure 1E; $F_{2,23}$ = 8.358, p = 0.002, for one-way analysis of variance [one-way ANOVA]; stimulation condition main effect; NoSTIM versus IN: p = 0.001, NoSTIM versus OUT: p = 0.438, and IN versus OUT: p = 0.007, Fisher's least significant difference [LSD]). Collectively, these results demonstrate that spindles are not effective per se, but instead enhance hippocampus-dependent memory only if they coincide with the more excitable depolarizing up-state of a slow oscillation (Bergmann et al., 2012; Chauvette et al., 2012). Neither in-phase nor out-of-phase stimulation changed memory for cued fear compared with that observed in no-stimulation control mice ($F_{2,23}$ = 0.051, p = 0.950), indicating that our stimulation in-phase during NREM sleep preferentially benefits hippocampus-dependent memory (Cai et al., 2009).

The hippocampal dependency of the effect of in-phase spindle stimulation was assured in 26 additional mice using an object-place recognition task (OPR; Figure S2) known to be sensitive to the effects of sleep (Binder et al., 2012). Mice receiving stimulation in-phase with the slow oscillation up-state during slow wave sleep (SWS) after learning showed enhanced place memory (in terms of enhanced exploration time for the displaced object) on retrieval testing 24 hr later ($F_{2,23}$ = 4.338, p = 0.025; Figure S2C). Place memory after out-of-phase stimulation did not differ from memory in the no-stimulation control group. Together, these results suggest that spindle stimulation phase-locked to the slow oscillation up-state specifically enhances consolidation of hippocampus-dependent memory during sleep.

Enhancing Effects of In-Phase Stimulation on Slow Oscillation-Spindle Coupling and Contextual Memory Occur in the Absence of Alteration in Sleep Architecture

The effects of in-phase stimulation on memory formation were not conveyed by gross changes in sleep architecture. Sleep onset and time spent in different sleep stages during the 6 hr interval were closely comparable among the three stimulation conditions (Table S1). Also, the overall density of slow oscillation, spindle, and ripple events did not differ among conditions (Table S2). However, optogenetic spindle stimulation altered the fine-tuned interplay between the three rhythms (Figure 2A). Averaging electroencephalograms (EEGs), time-locked to stimulation onsets, confirmed the emergence of spindle-like activity coalescing with a large negative slow oscillation half-wave during in-phase stimulation; notably, this negative half-wave was absent in the out-of-phase condition (Figure 2B). Moreover, this analysis revealed that the optogenetic spindle-like generation of the anterior TRN induced predominantly frontal cortex (FRO) spindles, which, on average, synchronized to the stimulation. An entrainment by

the optogenetic stimulation was also observed for spindles in the hippocampal CA1 region, which is consistent with observations that spindles invade hippocampal structures (Sarasso et al., 2014; Sullivan et al., 2014). However, surprisingly, spindle-like stimulation did not entrain spindles recorded in parietal cortex (PAR). Overall, this distribution indicates that the stimulated TRN regions mediate a specific topographical pattern of spindle activity and influence the hippocampal local field potential within short delays.

Determining discrete spindle events within a 750 ms time window following the onset of stimulation revealed for FRO recordings a significantly higher spindle incidence rate for in-phase than out-of-phase stimulation conditions (Figure 3A, left; one-way ANOVA, $F_{3,36}$ = 60.243, $p < 0.001$; IN versus OUT: $p < 0.001$, Fisher's LSD), as well as a distinct elevation compared with the corresponding no-stimulation conditions, no-stimulation in-phase (IN versus NoSTIM-IN: $p < 0.001$, Fisher's LSD), and no-stimulation out-of-phase conditions (OUT versus NoSTIM-OUT: $p < 0.001$, Fisher's LSD). Increases in spindle incidence were closely comparable between in-phase and out-of-phase stimulation with reference to the rates during the respective NoSTIM-IN and NoSTIM-OUT control conditions. In the NoSTIM-IN condition, spindle density within 750 ms following detection of a slow oscillation up-state was significantly higher than that for the delayed interval corresponding to the out-of-phase stimulation protocol (NoSTIM-OUT versus NoSTIM-IN: $p < 0.001$, Fisher's LSD; Figure 3A), confirming endogenous phase-locking between slow oscillations and spindles. No difference was found for the incidence of PAR and CA1 spindles following stimulation or slow oscillation detection (one-way ANOVA, PAR: $F_{3,36}$ = 1.275, $p = 0.297$; CA1: $F_{3,36}$ = 0.615, $p = 0.610$). Importantly, whereas the ratio of the total spindle count to the total slow oscillation count (for the 6 hr period of sleep monitoring) was comparable in all three conditions (Figure 3B; Kruskal-Wallis one-way ANOVA, U_2 = 3.640, $p = 0.162$), slow oscillation-spindle coupling (i.e., the proportion of detected slow oscillations that are coupled with a spindle within 750 ms) was distinctly increased for the in-phase condition compared with both out-of-phase and no-stimulation conditions (Figure 3C; Kruskal-Wallis one-way ANOVA, U_2 = 16.923, $p < 0.001$). Time-event correlation histograms also confirmed that spindle modulation during optogenetic stimulation, as observed not only in the cortical EEG but also in local field potential (LFP) recordings from CA1, derives from spindle cycles that are highly synchronized to the imposed stimulation rhythm (Figure 3D), with this synchrony being absent in the no-stimulation condition. Finally, we examined the influence of the TRN stimulation on inter-event intervals by determining the spindle incidence for a time window of 1.5 to 2 s post-stimulus. This analysis did not reveal any persisting effect on the generation of spindles ($F_{3,36} < 1.170$, $p > 0.170$).

Out-of-Phase Stimulation, Unlike In-Phase Stimulation, Induces Slow Oscillations without Affecting Memory Consolidation

We then asked whether thalamic spindle stimulation exerts a bottom-up effect on cortical slow oscillations. Averaging EEG responses filtered in the 0.5–4.0 Hz band time-locked to stimulation onset did not reveal any difference in amplitude of slow oscillations occurring during in-phase stimulation and the corresponding interval of the no-stimulation condition (Table S3), excluding an immediate effect of in-phase stimulation on ongoing slow oscillation activity. However, an analysis of slow oscillation negative half-wave peaks in the FRO within a 500 ms interval following stimulus onset (Figure 4A) revealed a distinctly increased probability of the emergence of a slow oscillation during this interval in the out-of-phase condition compared with all other conditions (Figure 4B), including a comparison with an interval of the no-stimulation condition that covered the respective out-of-phase stimulation period (one-way ANOVA, $F_{3,36}$ = 76.356, $p < 0.001$; OUT versus NoSTIM-OUT: $p < 0.001$, Fisher's LSD). The stimulation-induced slow oscillations emerged mainly during the first 250 ms of the out-of-phase spindle stimulation (Figure 4C, top right), but not in-phase spindle stimulation (Figure 4C, top left). The enhancing effect of out-of-phase stimulation on slow oscillation incidence was also found to be significant in the PAR region (one-way ANOVA, $F_{3,36}$ = 15.277, $p < 0.001$; OUT versus NoSTIM-OUT: $p = 0.011$, Fisher's LSD). In control analyses, we confirmed that out-of-phase stimulation was performed without a particular phase preference to continuing or newly appearing slow oscillation (Figure S4), whereas in-phase stimulation was consistently performed during a slow oscillation up-state (Figure S4). Overall, these results indicate that spindle stimulation of the TRN can induce slow oscillations in the out-of-phase condition but did not affect the consolidation of contextual memory in this group compared with the no-stimulation control group.

Optogenetically Induced Spindles Preserve Natural Hippocampal Nesting and Enhance Memory via Triple Coupling of Slow Oscillations, Spindles, and Ripples

We next examined whether spindles induced optogenetically using our protocols are similar to spontaneous spindles in terms of their influence on hippocampal oscillations (Figures S5A and S5B). Previous studies have shown a high propensity for sleep spindles to synchronize hippocampal ripples into their troughs (Clemens et al., 2011; Phillips et al., 2012) (Figure 5A). A nesting of ripple activity into the troughs of the spindle cycle in particular for spindles recorded at PAR and CA1 (Figures S5C and S5D) was observed and was closely comparable among all stimulation conditions, as confirmed by more fine-grained time-event correlation histograms of discrete ripple events time-locked to the spindle troughs (Figure S5C; $p < 0.001$). Consistent with findings in humans and rodents (Clemens et al., 2011; Phillips et al., 2012), grouping of ripples to spindle troughs was evident for parietal cortical and hippocampal spindles (Figure S5D) but was absent during frontal spindles. This result indicates that the spindle stimulation did not affect the naturally weak spindle-ripple nesting in FRO recordings and mostly preserved known nesting properties of CA1 ripples into PAR and CA1 spindles troughs.

We found that optogenetic stimulation did not affect the ripple incidence rate under any condition (Figure 5B; one-way ANOVA, $F_{3,30}$ = 1.258, $p = 0.306$). However, an analysis of the temporal overlap of spindle and ripple events revealed that the proportion of hippocampal ripples co-occurring with spindle events during optogenetic stimulation was increased in the in-phase

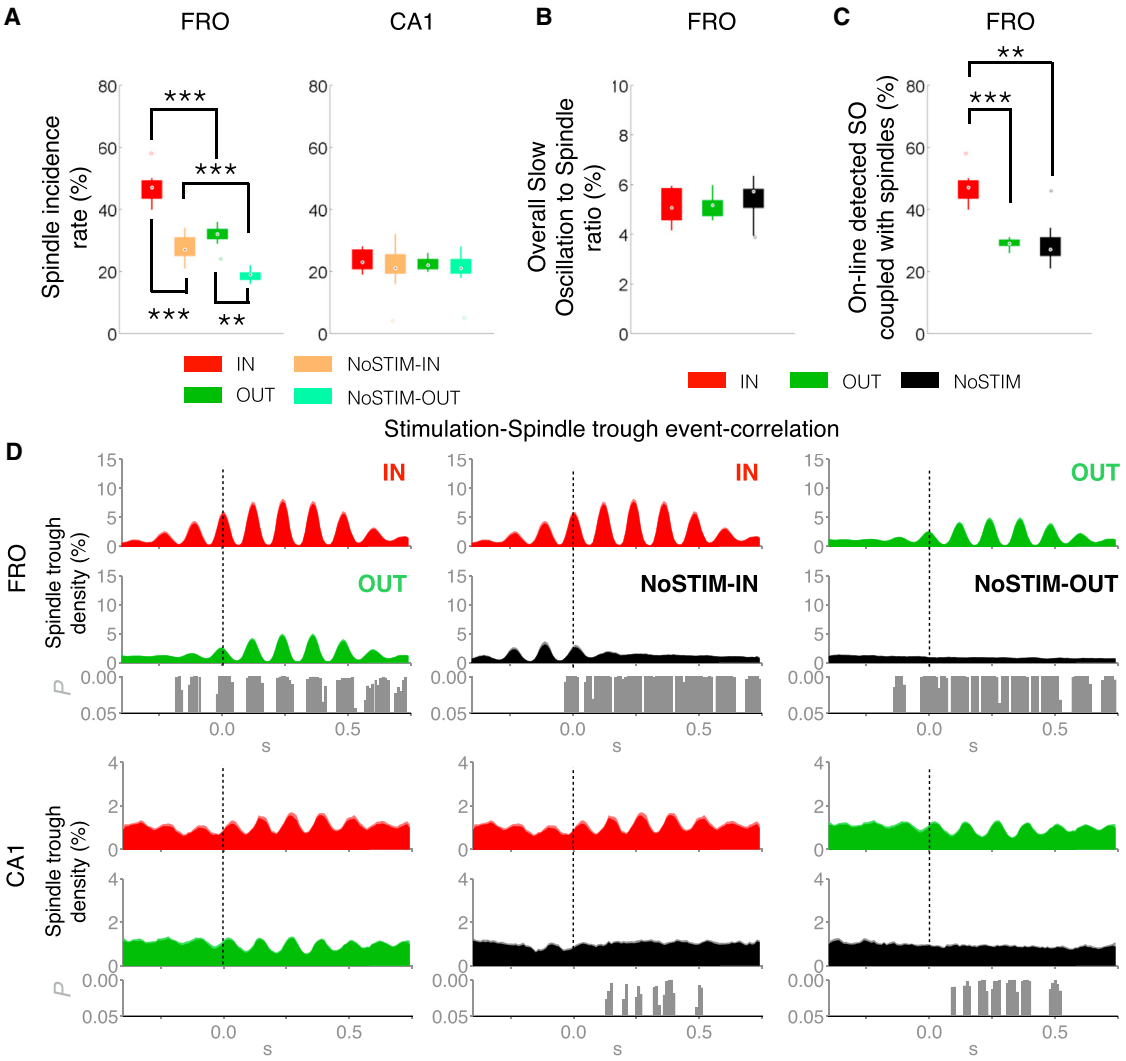

Figure 3. In-Phase Stimulation Increases Spindle Incidence

(A) Spindle incidence rate (in percent of total stimulations) in frontal (FRO, left) and hippocampal (CA1, right) recordings following in-phase (IN, red) and out-of-phase (OUT, green) stimulation and for the corresponding periods in the respective no-stimulation control conditions (NoSTIM-IN, orange; NoSTIM-OUT, light green). An induced spindle was defined as a spindle event occurring within a 750 ms interval following the start of stimulation.

(B) The ratio (set to 100%) of the total number of spindles to that of slow oscillations identified offline during the entire 6 hr sleep period for in-phase (red bar), out-of-phase (green bar), and no-stimulation (black bar) groups.

(C) Proportion of online-detected slow oscillations which coincided with a spindle within 750 ms after slow oscillation detection for in-phase (red bar), out-of-phase (green bar), and no-stimulation conditions (black bar). ***$p < 0.001$, **$p < 0.01$ for post hoc pairwise comparisons; data in (A)–(C) are shown as box-whisker plots with box limits representing the first and third quartile and whiskers indicating the data range.

(D) Means ± SEMs for event-correlation histogram of identified spindle troughs in frontal EEG (FRO, top) and hippocampal LFP recordings (CA1, bottom), time-locked to stimulation onset (t = 0) for in-phase (IN, red histogram), out-of-phase (OUT, green), and corresponding no-stimulation control conditions (NoSTIM, black). The spindle trough density percentage was estimated as the number of detected spindle troughs per 10 ms bin, divided by the total number of stimulations during the 6 hr intervention (set to 100%). Left column: comparison of in-phase and out-of-phase stimulation. Middle and right columns: comparison of in-phase (middle) and out-of-phase (right) stimulation with corresponding periods of the no-stimulation control. Significant differences (p values) are indicated at the bottoms of panels.

stimulation condition (one-way ANOVA, $F_{3,30} = 14.679$, $p < 0.001$) compared with the no-stimulation condition (Figure 5C; NoSTIM-IN versus IN: $p = 0.001$ and NoSTIM-OUT versus OUT: $p = 0.162$, Fisher's LSD). Notably, 20% of induced spindles were accompanied by a ripple, with no significant difference among conditions (one-way ANOVA, $F_{3,30} = 1.277$, $p = 0.3$). Importantly, the percentage of online-detected slow oscillations co-occurring with a spindle (within 750 ms after detection) that also exhibited at least one ripple co-occurring within a spindle was significantly increased in the in-phase group compared to the no-stimulation and out-of-phase groups (Figure 5D; Kruskal-Wallis one-way ANOVA, $U_2 = 9.974$, $p = 0.007$; NoSTIM versus IN: $p = 0.024$,

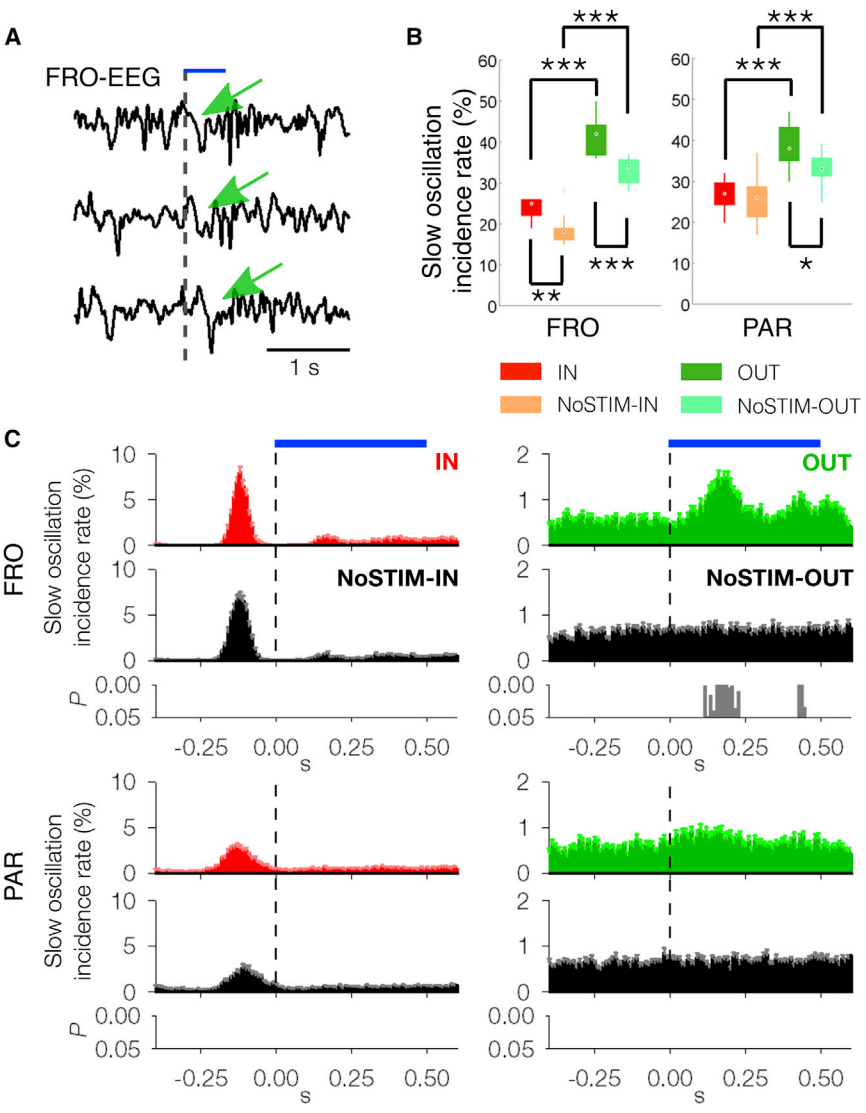

Figure 4. In-Phase Spindle-like Stimulation Does Not Affect the Occurrence of Slow Oscillations, whereas Out-of-Phase Stimulation Does

(A) Three representative 3.5 s traces of frontal EEG recordings illustrating slow oscillations evoked by out-of-phase stimulation (marked by green arrows). Dashed vertical line indicates the beginning of the stimulation period (horizontal blue bar).

(B) Slow oscillation incidence rate in frontal (FRO, left) and parietal (PAR, right) following in-phase (IN, red) and out-of-phase (OUT, green) stimulation and the corresponding no-stimulation control conditions (NoSTIM-IN, orange; NoSTIM-OUT, light green). ***p < 0.001, **p < 0.01, *p < 0.05 for post hoc pairwise comparisons; data are shown as box-whisker plots with box limits representing the first and third quartile and whiskers representing the minimum and maximum range of the data.

(C) Mean ± SEM event-correlation histogram of slow oscillation events (slow oscillation incidence rate, defined as the number of detected slow oscillation events, characterized by their negative peaks, divided by the total number of stimulations during the 6 hr intervention) in EEG recordings over frontal (FRO, top) and parietal (PAR, bottom) cortical areas, time-locked to stimulation onset for in-phase (left, red) and out-of-phase (right, green) stimulation and their respective no-stimulation control periods (NoSTIM-IN and NoSTIM-OUT, black). Horizontal blue bar indicates stimulation interval. Note that the distinct increase in frontal slow oscillation events during out-of-phase stimulation concentrated at 0.1–0.25 s post-stimulation onset.

NoSTIM versus OUT: p = 0.372, and IN versus OUT: p = 0.002, Fisher's LSD).

Since sleep spindles are known to be spatially distributed oscillations, we further examined the cross regional occurrence of spindles during stimulation. In-phase stimulation was accompanied by a significant increase in the rate of co-occurring (i.e., temporally overlapping) spindle events between FRO and PAR recordings ($F_{2,22} = 13.298$, $p < 0.001$, one-way ANOVA), between FRO and CA1 recordings ($F_{2,13.337} = 6.602$, p = 0.010, Welch test), and between all three recording sites (FRO-PAR-CA1, $U_2 = 7.175$, p = 0.028, Kruskal-Wallis one-way ANOVA) compared to the out-of-phase and no-stimulation conditions (Figure S6). We further examined whether these coherent spindle events also included a hippocampal ripple. Consistent with the increase in (detected) slow oscillation, frontal spindle, and hippocampal ripple events during in-phase stimulation (reported above; Figure 5D), this analysis showed that in-phase stimulation, in comparison with the other two conditions, was specifically associated with an increased rate of coherent frontal-hippocampal spindle events, including a ripple (Figure 5E; $U_2 = 13.008$, p = 0.001, Kruskal-Wallis one-way ANOVA; IN versus NoSTIM: p = 0.004, IN versus OUT: p = 0.001, and OUT versus NoSTIM: p = 0.605; rank-sum test). In sum, these results indicate that in-phase stimulation produces a unique temporal-spatial pattern of the three oscillatory phenomena of interest, characterized not only by an increased triple coupling of slow oscillation, spindle, and ripple events, but also by an increased co-occurrence of spindles in anterior and posterior cortical and hippocampal regions, where, in particular, spindles co-occurring in frontal cortex and hippocampus also entrain ripples.

Optogenetic Inhibition In-Phase Induces Impairment of Contextual Memory Consolidation

We finally tested whether optogenetic inhibition of TRN Prv neurons could affect memory formation. Prv-cre knockin mice were bilaterally injected in the TRN (Figure 6A) with pAAV-CBA-Flex-Arch-GFP (Figures 6B–6E). Mice were subjected to stimulation protocols corresponding to in-phase optogenetic inhibition (IN-ARCH; 500 ms yellow laser pulse following the detection of a slow oscillation up-state; n = 8), out-of-phase optogenetic inhibition (OUT-ARCH; 500 ms yellow laser pulse randomly given

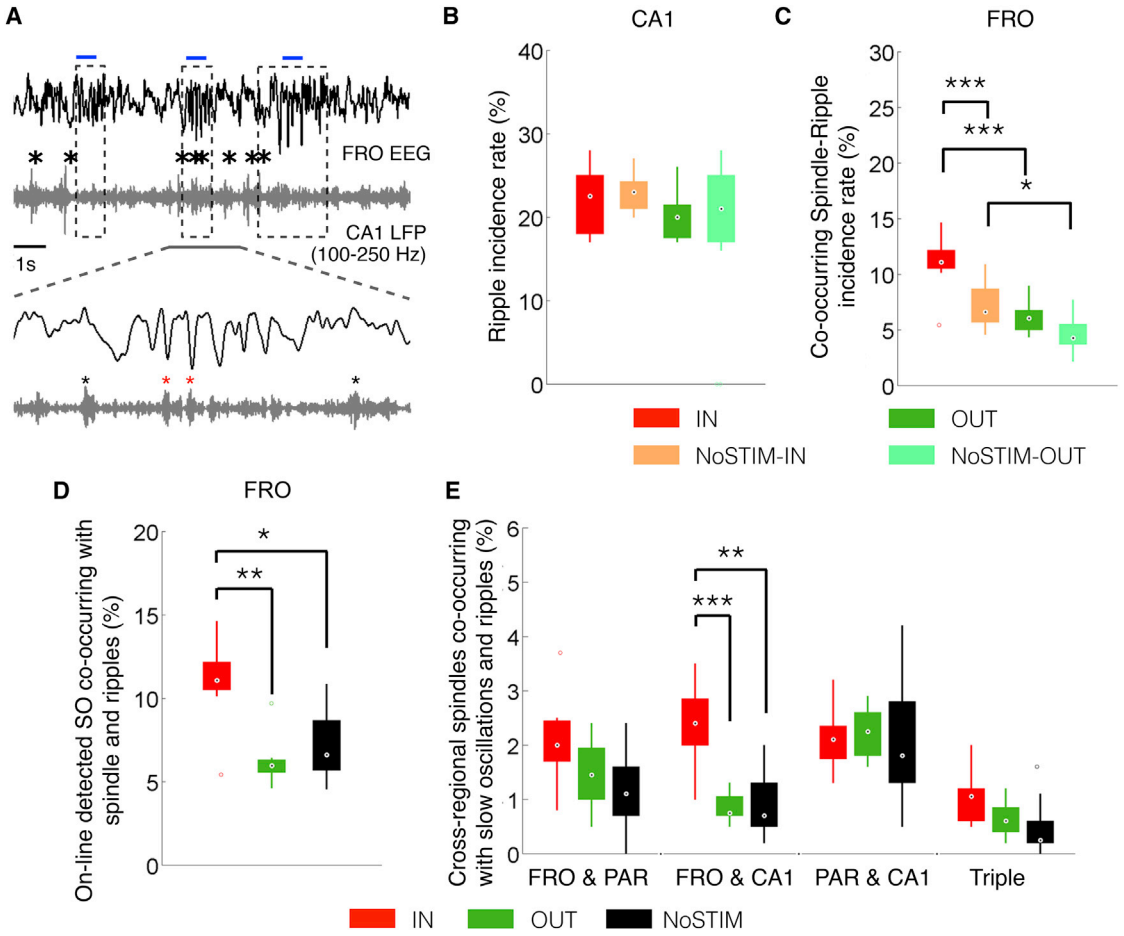

Figure 5. Effects of the Stimulation on Hippocampal Ripples and Cross Regional Spindles Co-occurring with Slow Oscillations and Spindles

(A) Representative 10 s traces of raw frontal (FRO) EEG and hippocampal (CA1) LFP recordings filtered between 100 and 250 Hz. Periods with discrete spindle events in the EEG are framed by dashed lines. Black asterisks indicate CA1 ripple events. Below is a magnification of the second detected spindle, illustrating ripples coinciding with spindles (red asterisks) during light stimulation (blue bars).

(B) CA1 ripple incidence rate (in percent of stimulations) induced by in-phase (red) and out-of-phase (green) optogenetic stimulation and the corresponding periods for no-stimulation controls (NoSTIM-IN, orange; NoSTIM-OUT, light green). An induced ripple was defined as a ripple event occurring 750 ms after stimulation onset.

(C) Proportion of hippocampal ripples co-occurring with FRO spindles following in-phase (IN, red) and out-of-phase (OUT, green) stimulation and the corresponding periods for no-stimulation controls (NoSTIM-IN, orange; NoSTIM-OUT, light green).

(D) Proportion (per online detected slow oscillations) of frontal spindles co-occurring with at least one hippocampal ripple within 750 ms following an online detected slow oscillation (which corresponds to the proportion of slow oscillations-spindle-ripples triples) for in-phase (IN, red bar), out-of-phase (OUT, green bar), and no-stimulation control conditions (NoSTIM, black).

(E) Incidence rate (in percent of total number of stimulations) of offline detected spindle events co-occurring in frontal and parietal (FRO & PAR), frontal and hippocampal (FRO & CA1), parietal and hippocampal (PAR & CA1), or all three recording sites (triple) and with at least one hippocampal ripple event within 750 ms following stimulation onset. ***$p < 0.001$, **$p < 0.01$, *$p < 0.05$ for post hoc pairwise comparisons; data are shown as box-whisker plots with box limits representing the first and third quartile and whiskers indicating the data range.

between 0.5 to 1.0 following the detection of a slow oscillation up-state; n = 7), or no-stimulation condition (NoSTIM; no laser stimulation given; n = 9). We found that in-phase optogenetic inhibition of Prv neurons resulted in a significantly lower contextual memory recall (Figure 6F; one-way ANOVA, $F_{2,23}$ = 5.665, p = 0.011) compared to the no-stimulation group (IN-ARCH versus NoSTIM: p = 0.043, Fisher LSD) or OUT-ARCH group (IN-ARCH versus OUT-ARCH: p = 0.003, Fisher's LSD). The out-of-phase TRN inhibition did not significantly affect memory (NoSTIM versus OUT-ARCH: p = 0.199, Fisher's LSD). The tone recall was not significantly changed (one-way ANOVA, $F_{2,23}$ = 3.304, p = 0.057).

As expected, the spindle incidence rate was significantly reduced for the mice that received inhibitory TRN stimulation if compared to the respective no-stimulation control conditions (Figure 6G; $F_{3,25}$ = 12.042, p = 0.001, one-way ANOVA, IN versus NoSTIM-IN: p = 0.035, and OUT versus NoSTIM-OUT: p = 0.015). In line with our findings from the main experiments demonstrating that a spindle-like stimulation of the TRN induced slow oscillations, the inhibitory manipulation significantly reduced

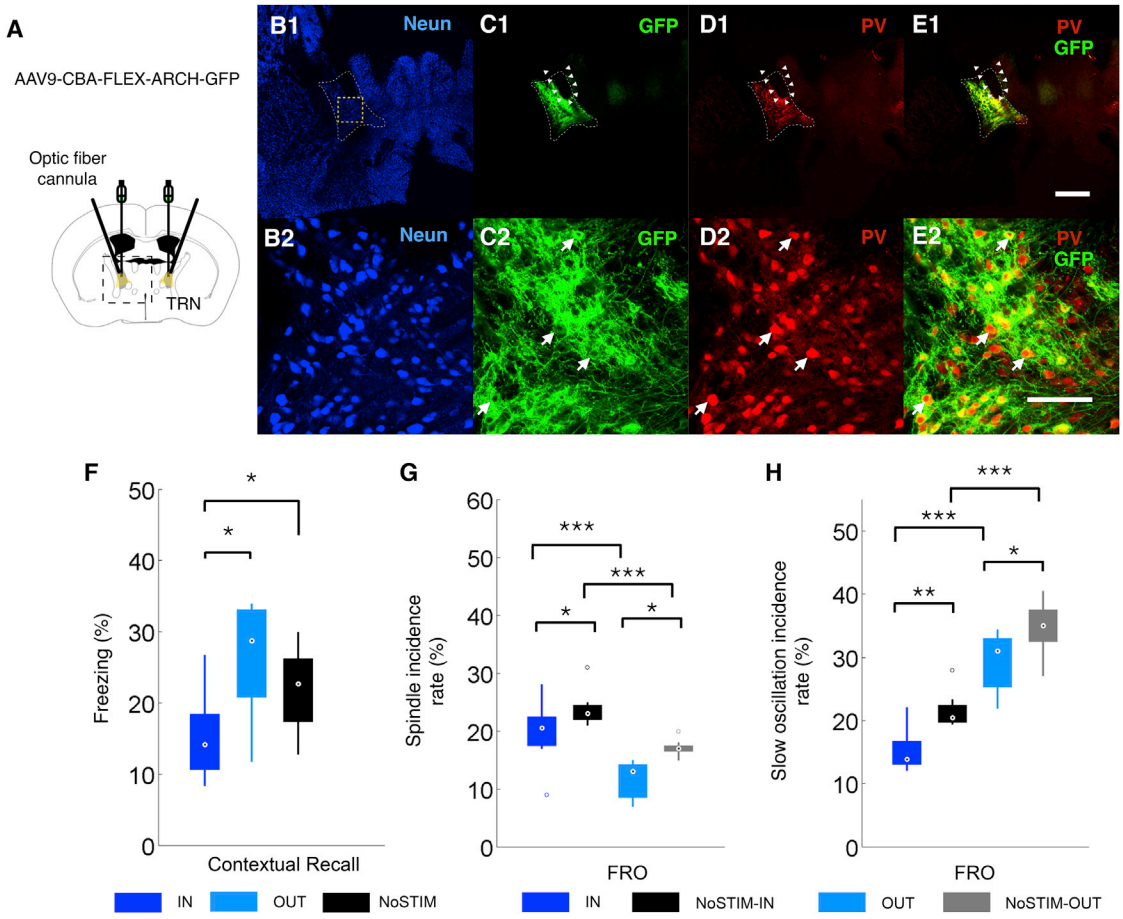

Figure 6. Inhibition of the TRN In-Phase with Slow Oscillation Up-States Impairs Contextual Memory

(A) Schematic showing a typical coronal section used for bilateral injection of pAAV-CBA-Flex-Arch-GFP.WPRE.SV40 virus and the implantations scheme of optic fiber cannula in the TRN of Prv-cre knockin mice.

(B1–E1) Representative coronal section of the thalamus stained against NeuN antibody (B1), viral expression of ARCH-GFP virus in the TRN region (C1), staining against PV antibody (D1), and merged ARCH-GFP/PV staining (E1). Scale bar represents 100 μm.

(B2–E2) Magnification of the area marked by the white dashed square in (B1) for the corresponding staining/fluorescence as shown in (B1)–(F1). Scale bar represents 100 μm.

(F) Contextual fear memory (Freezing %) following in-phase inhibition (IN-ARCH; n = 8, blue), out-of-phase inhibition (OUT-ARCH; n = 7, light blue), and no-stimulation (NoSTIM; n = 9, black).

(G) Spindle incidence rate (as percentage of total number of stimulations) in frontal (FRO) recordings following TRN inhibition in-phase (blue) and out-of-phase (light-blue) with detected slow oscillation and their corresponding control conditions (NoSTIM-IN, black; NoSTIM-OUT, gray).

(H) Slow oscillation incidence rate (in percent of the total number of stimulations) in frontal recordings during in-phase (IN, blue), out-of-phase (OUT, light-blue), and no-stimulation conditions (NoSTIM-IN, black; NoSTIM-OUT, gray). Incidence rates were determined by the number of spindles/slow oscillations occurring within a 750 ms interval following the onset of the inhibitory stimulus and normalized by the total number of stimulations. ***$p < 0.001$, **$p < 0.01$, *$p < 0.05$ for post hoc pairwise comparisons; data are shown as box-whisker plots with box limits representing the first and third quartile and whiskers indicating the data range.

the incidence of slow oscillations during the 750 ms post-stimulus window for the in-phase and out-of-phase stimulation conditions, in comparison with their respective control conditions (Figure 6H; $F_{3,25} = 23.921$, $p < 0.001$, one-way ANOVA, IN versus NoSTIM-IN: p = 0.002, OUT versus NoSTIM-OUT: p = 0.019). Inhibitory stimulation had no effect on incidence rates of hippocampal ripples (one-way ANOVA, $F_{3,25} = 2.151$, p = 0.121; data not shown).

Finally, to ensure that the promoting effect of spindle-like in-phase TRN stimulation on hippocampal-dependent memory is specific to the stimulation frequency, we performed another control experiment utilizing TRN stimulation at 20 Hz (i.e., a frequency unrelated to the spindle band) in mice expressing ChR2 (n = 7) and in control mice expressing YFP (n = 10; please see legend of Figure S7 and STAR Methods for details). Comparison between these two groups showed no difference in contextual fear memory ($F_{1,15} = 0.017$, p = 0.899; Figure S7F) or spindle incidence in the 750 ms post-stimulus interval (FRO: $F_{1,15} = 1.361$, p = 0.262; Figure S7D).

Together, these results confirm that a modulation of the TRN activity coinciding with a slow oscillation up-state and preeminently frequency-specific to the spindle range, with a combined impact on spindle and slow oscillation incidence, is important for hippocampal memory consolidation during sleep.

DISCUSSION

By combining optogenetics with a closed-loop stimulation approach (Grosenick et al., 2015), our experiments provide evidence for an essential role that the thalamus plays in memory consolidation during sleep through its coordinating influence on the interplay between the three rhythms involved in this memory process.

Memory formation during sleep involves the replay of hippocampal representations during ripples (Diba and Buzsáki, 2007; Girardeau et al., 2009; Wilson and McNaughton, 1994), which is thought to promote systems consolidation, i.e., the passage of the reactivated information mainly toward neocortical regions that serve as long-term storage sites (Diekelmann and Born, 2010; Dudai et al., 2015). In this hypothesis, the phase coupling of ripples, spindles, and slow oscillations is thought to mediate effective hippocampal-to-neocortical information transmission. Our report here provides experimental evidence that the phase coupling of the three rhythms essentially contributes to effective memory consolidation during sleep. Moreover, our studies have uncovered a key contribution of spindles to coordinating the interplay between the three rhythms involved in this memory process.

We found that thalamic-induced spindles nest hippocampal ripples to their troughs both in optogenetically induced and spontaneous conditions. This pattern suggests that spindles, rather than slow oscillations, are the major factor synchronizing the occurrence of hippocampal ripples and possibly memory replay, in the first place, to the excitable phase of the spindle cycle and, in the case of slow oscillation driven spindles, to the excitable slow oscillation up-states (Clemens et al., 2007; Isomura et al., 2006; Sirota et al., 2003; Staresina et al., 2015). Whereas the mechanism of spindle oscillation-induced nesting of ripples remains unclear, our results support the view that the increased spindle-ripple co-occurrence in the presence of a slow oscillation up-state represents a condition promoting the systems consolidation of contextual memory. Indeed, given that ripples enwrap reactivated hippocampal memory information, our observations are consistent with the notion of spindle-ripple events facilitating the hippocampal-to-neocortical transmission of memory information for longer-term storage in neocortical networks (Buzsáki, 1998; Dudai et al., 2015).

Taking this systems consolidation perspective, our finding is of interest that in-phase stimulation appeared to increase spindles phase-locked to slow oscillations mainly over frontal cortical regions, whereas nesting of ripples within spindle troughs revealed to be stronger for parietal cortical and hippocampal networks, a pattern which has been likewise revealed to occur spontaneously under unstimulated conditions in humans (Clemens et al., 2011). Simultaneously, in-phase stimulation increased the co-occurrence of spindles between frontal and parietal cortical regions as well as between frontal as hippocampal sites. Taken together, this topographical pattern suggests that the putative hippocampal-to-neocortical transmission of reactivated memory information during spindle-ripple events involves a fine-tuning between anterior and posterior spindle activities in thalamo-cortical networks, with the former primarily impacting frontal cortical networks and the later primarily serving to synchronize memory reactivations in hippocampal networks. While this fine-tuning of spindle activities and its function remains to be elucidated, we speculate that the frontal spindles are particularly relevant for redistributing the representation toward respective neocortical networks. This view is supported by our finding that the enhancing influence of in-phase stimulation on the incidence of slow oscillation-spindle-ripple triplets was specifically linked to the frontal cortical recordings. Generally, spindles that occur during the excitable up-state of the slow oscillation can be considered to be particularly effective in inducing plastic synaptic changes in cortical networks that mediate the more persistent storage of the memory information in neocortical networks (Chauvette et al., 2012; Rosanova and Ulrich, 2005; Sejnowski and Destexhe, 2000).

Moreover, the view of slow oscillation-spindle-ripple triplets reflecting systems consolidation of hippocampal memories, in light of our findings, implicates that silencing frontal cortex during sleep within 6 hr after fear conditioning should impair memory consolidation which, at a first glance, contrasts with the rather slow temporal gradient in which memories become independent of the hippocampus (Frankland and Bontempi, 2005). However, although a direct test of this implication is missing, there is evidence that, depending on pre-existing knowledge, new memories can become rather quickly independent from hippocampus (within 24 hr) and at this stage can be also disrupted by impairing prefrontal cortex function (e.g., Lesburguères et al., 2011; Tse et al., 2007, 2011).

In addition, we found that the thalamic-induced spindle-like stimulation can promote the generation of a cortical slow oscillation, whereas an inhibition of the TRN resulted in a reduced incidence of slow oscillations. Here, we confirmed that the effect on slow oscillation incidence alone was not sufficient to alter the consolidation of memory since enhancing versus suppressing slow oscillation events in the respective out-of-phase conditions did not express itself in corresponding changes in memory performance. Although a contribution of TRN activation to the emergence of slow oscillations has been reported by others (Lewis et al., 2015), our findings are the first to show that TRN stimulation that mimics natural thalamo-cortical spindle input suffices to generate a cortical slow oscillation. The mechanisms mediating this effect remain obscure. The effect might reflect a phase-resetting of cortical networks, which spindles produce by facilitating the transition of network activity into the slow oscillation down-states. However, a mere resetting would not explain that spindles induced out-of-phase increased the absolute number of slow oscillation events. The state of readiness of TRN neurons, i.e., the number of recruitable neurons for population spiking, and on-going thalamo-cortical oscillations might be another factor determining whether stimulation produces spindles (Barthó et al., 2014) together with slow oscillations (Lewis et al., 2015) or no

response. In natural conditions, thalamo-cortical spindle activity might contribute to the development of longer trains of slow oscillatory activity (Mölle et al., 2011; Ngo et al., 2015).

Importantly, we found that both in-phase and out-of-phase inhibition of TRN reduced the occurrence of spindles; however, only mice subjected to an in-phase inhibition of the TRN showed an impairment during contextual fear recall, corroborating the view that a reduction in spindles alone is not sufficient to disrupt memory formation. Instead, an effective impairment requires that the inhibition of spindles occurs in the presence of a cortical slow oscillation up-state, obviously representing the time window during which, under normal conditions, the hippocampal-cortical dialog underlying systems consolidation is vulnerable.

It might be argued that the effect of TRN stimulation was unspecific and not dependent on the spindle-like stimulation protocol employed in the main experiment. This was ruled out by a control study where tonic (500 ms) stimulation of the TRN at 20 Hz did not show any effect on both contextual fear memory and the coupling of spindles, thus supporting the specificity of the reported effects for the applied stimulation protocol. Altogether, the emerging picture challenges the view that phase coupling of NREM sleep rhythms and associated memory formation is under the sole or primary control of the cortical slow oscillation (Cox et al., 2012; Diekelmann and Born, 2010; Steriade, 2006), instead revealing a critical contribution of thalamic spindles to this process.

STAR★METHODS

Detailed methods are provided in the online version of this paper and include the following:

- KEY RESOURCES TABLE
- CONTACT FOR REAGENT AND RESOURCE SHARING
- EXPERIMENTAL MODEL AND SUBJECT DETAILS
  - Mice
- METHOD DETAILS
  - Surgery
  - Histology
  - Procedure and Design
  - Contextual Fear Conditioning
  - Object Place Recognition Task
  - Electrophysiological Recordings and Closed-Loop Optogenetic Stimulation Setup
- QUANTIFICATION AND STATISTICAL ANALYSIS
  - Analyses of Sleep Measures and EEG
  - Evoked Potentials
  - Offline Detection of Sleep Spindles, Ripples, and Slow Oscillations
  - Statistical Analysis
- DATA AND SOFTWARE AVAILABILITY

SUPPLEMENTAL INFORMATION

Supplemental Information includes seven figures and five tables and can be found with this article online at http://dx.doi.org/10.1016/j.neuron.2017.06.025.

AUTHOR CONTRIBUTIONS

C.-F.V.L. and H.-V.V.N. performed the experiments and analysis. C.-F.V.L., H.-V.V.N., J.B., and H.-S.S. designed the experiment and wrote the manuscript.

ACKNOWLEDGMENTS

This work was supported by the grant IBS-R001-D1 from the Institute for Basic Science, Korea, the Deutsche Forschungsgemeinschaft (Tr-SFB 654 "Plasticity and Sleep"), and the German Federal Ministry of Education and Research (01GI0925 and 01GQ0973). We thank Matthias Mölle, Eunyoung Bang, Boyoung Lee, Yooncheol Jang, Joon-Hyuk Lee, and Seung-eun Lee for experimental support.

Received: December 19, 2016
Revised: May 7, 2017
Accepted: June 15, 2017
Published: July 6, 2017

REFERENCES

Aeschbach, D., and Borbély, A.A. (1993). All-night dynamics of the human sleep EEG. J. Sleep Res. *2*, 70–81.

Asrican, B., Augustine, G.J., Berglund, K., Chen, S., Chow, N., Deisseroth, K., Feng, G., Gloss, B., Hira, R., Hoffmann, C., et al. (2013). Next-generation transgenic mice for optogenetic analysis of neural circuits. Front. Neural Circuits *7*, 160.

Barthó, P., Slézia, A., Mátyás, F., Faradzs-Zade, L., Ulbert, I., Harris, K.D., and Acsády, L. (2014). Ongoing network state controls the length of sleep spindles via inhibitory activity. Neuron *82*, 1367–1379.

Bergmann, T.O., Mölle, M., Schmidt, M.A., Lindner, C., Marshall, L., Born, J., and Siebner, H.R. (2012). EEG-guided transcranial magnetic stimulation reveals rapid shifts in motor cortical excitability during the human sleep slow oscillation. J. Neurosci. *32*, 243–253.

Binder, S., Baier, P.C., Mölle, M., Inostroza, M., Born, J., and Marshall, L. (2012). Sleep enhances memory consolidation in the hippocampus-dependent object-place recognition task in rats. Neurobiol. Learn. Mem. *97*, 213–219.

Boyce, R., Glasgow, S.D., Williams, S., and Adamantidis, A. (2016). Causal evidence for the role of REM sleep theta rhythm in contextual memory consolidation. Science *352*, 812–816.

Buzsáki, G. (1998). Memory consolidation during sleep: a neurophysiological perspective. J. Sleep Res. *7* (*Suppl 1*), 17–23.

Buzsáki, G., Horváth, Z., Urioste, R., Hetke, J., and Wise, K. (1992). High-frequency network oscillation in the hippocampus. Science *256*, 1025–1027.

Cai, D.J., Shuman, T., Gorman, M.R., Sage, J.R., and Anagnostaras, S.G. (2009). Sleep selectively enhances hippocampus-dependent memory in mice. Behav. Neurosci. *123*, 713–719.

Chauvette, S., Seigneur, J., and Timofeev, I. (2012). Sleep oscillations in the thalamocortical system induce long-term neuronal plasticity. Neuron *75*, 1105–1113.

Chow, B.Y., Han, X., Dobry, A.S., Qian, X., Chuong, A.S., Li, M., Henninger, M.A., Belfort, G.M., Lin, Y., Monahan, P.E., and Boyden, E.S. (2010). High-performance genetically targetable optical neural silencing by light-driven proton pumps. Nature *463*, 98–102.

Clemens, Z., Mölle, M., Eross, L., Barsi, P., Halász, P., and Born, J. (2007). Temporal coupling of parahippocampal ripples, sleep spindles and slow oscillations in humans. Brain *130*, 2868–2878.

Clemens, Z., Mölle, M., Eross, L., Jakus, R., Rásonyi, G., Halász, P., and Born, J. (2011). Fine-tuned coupling between human parahippocampal ripples and sleep spindles. Eur. J. Neurosci. *33*, 511–520.

Contreras, D., and Steriade, M. (1996). Spindle oscillation in cats: the role of corticothalamic feedback in a thalamically generated rhythm. J. Physiol. *490*, 159–179.

Cox, R., Hofman, W.F., and Talamini, L.M. (2012). Involvement of spindles in memory consolidation is slow wave sleep-specific. Learn. Mem. *19*, 264–267.

David, F., Schmiedt, J.T., Taylor, H.L., Orban, G., Di Giovanni, G., Uebele, V.N., Renger, J.J., Lambert, R.C., Leresche, N., and Crunelli, V. (2013). Essential thalamic contribution to slow waves of natural sleep. J. Neurosci. *33*, 19599–19610.

Diba, K., and Buzsáki, G. (2007). Forward and reverse hippocampal place-cell sequences during ripples. Nat. Neurosci. *10*, 1241–1242.

Diekelmann, S., and Born, J. (2010). The memory function of sleep. Nat. Rev. Neurosci. *11*, 114–126.

Dudai, Y., Karni, A., and Born, J. (2015). The consolidation and transformation of memory. Neuron *88*, 20–32.

Fogel, S.M., and Smith, C.T. (2011). The function of the sleep spindle: a physiological index of intelligence and a mechanism for sleep-dependent memory consolidation. Neurosci. Biobehav. Rev. *35*, 1154–1165.

Frankland, P.W., and Bontempi, B. (2005). The organization of recent and remote memories. Nat. Rev. Neurosci. *6*, 119–130.

Friedrich, M., Wilhelm, I., Born, J., and Friederici, A.D. (2015). Generalization of word meanings during infant sleep. Nat. Commun. *6*, 6004.

Gardner, R.J., Hughes, S.W., and Jones, M.W. (2013). Differential spike timing and phase dynamics of reticular thalamic and prefrontal cortical neuronal populations during sleep spindles. J. Neurosci. *33*, 18469–18480.

Girardeau, G., Benchenane, K., Wiener, S.I., Buzsáki, G., and Zugaro, M.B. (2009). Selective suppression of hippocampal ripples impairs spatial memory. Nat. Neurosci. *12*, 1222–1223.

Graves, L.A., Heller, E.A., Pack, A.I., and Abel, T. (2003). Sleep deprivation selectively impairs memory consolidation for contextual fear conditioning. Learn. Mem. *10*, 168–176.

Grosenick, L., Marshel, J.H., and Deisseroth, K. (2015). Closed-loop and activity-guided optogenetic control. Neuron *86*, 106–139.

Isomura, Y., Sirota, A., Özen, S., Montgomery, S., Mizuseki, K., Henze, D.A., and Buzsáki, G. (2006). Integration and segregation of activity in entorhinal-hippocampal subregions by neocortical slow oscillations. Neuron *52*, 871–882.

Khazipov, R., Sirota, A., Leinekugel, X., Holmes, G.L., Ben-Ari, Y., and Buzsáki, G. (2004). Early motor activity drives spindle bursts in the developing somatosensory cortex. Nature *432*, 758–761.

Kim, A., Latchoumane, C., Lee, S., Kim, G.B., Cheong, E., Augustine, G.J., and Shin, H.-S. (2012). Optogenetically induced sleep spindle rhythms alter sleep architectures in mice. Proc. Natl. Acad. Sci. USA *109*, 20673–20678.

Lesburguères, E., Gobbo, O.L., Alaux-Cantin, S., Hambucken, A., Trifilieff, P., and Bontempi, B. (2011). Early tagging of cortical networks is required for the formation of enduring associative memory. Science *331*, 924–928.

Lewis, L.D., Voigts, J., Flores, F.J., Schmitt, L.I., Wilson, M.A., Halassa, M.M., and Brown, E.N. (2015). Thalamic reticular nucleus induces fast and local modulation of arousal state. eLife *4*, e08760.

Logothetis, N.K., Eschenko, O., Murayama, Y., Augath, M., Steudel, T., Evrard, H.C., Besserve, M., and Oeltermann, A. (2012). Hippocampal-cortical interaction during periods of subcortical silence. Nature *491*, 547–553.

Maingret, N., Girardeau, G., Todorova, R., Goutierre, M., and Zugaro, M. (2016). Hippocampo-cortical coupling mediates memory consolidation during sleep. Nat. Neurosci. *19*, 959–964.

Marshall, L., Helgadóttir, H., Mölle, M., and Born, J. (2006). Boosting slow oscillations during sleep potentiates memory. Nature *444*, 610–613.

Mölle, M., Eschenko, O., Gais, S., Sara, S.J., and Born, J. (2009). The influence of learning on sleep slow oscillations and associated spindles and ripples in humans and rats. Eur. J. Neurosci. *29*, 1071–1081.

Mölle, M., Bergmann, T.O., Marshall, L., and Born, J. (2011). Fast and slow spindles during the sleep slow oscillation: disparate coalescence and engagement in memory processing. Sleep *34*, 1411–1421.

Morel, L., Higashimori, H., Tolman, M., and Yang, Y. (2014). VGluT1+ neuronal glutamatergic signaling regulates postnatal developmental maturation of cortical protoplasmic astroglia. J. Neurosci. *34*, 10950–10962.

Ngo, H.V., Martinetz, T., Born, J., and Mölle, M. (2013). Auditory closed-loop stimulation of the sleep slow oscillation enhances memory. Neuron *78*, 545–553.

Ngo, H.V., Miedema, A., Faude, I., Martinetz, T., Mölle, M., and Born, J. (2015). Driving sleep slow oscillations by auditory closed-loop stimulation-a self-limiting process. J. Neurosci. *35*, 6630–6638.

Paxinos, G., and Franklin, K. (2004). The Mouse Brain in Stereotaxic Coordinates (Gulf Professional Publishing).

Phillips, K.G., Bartsch, U., McCarthy, A.P., Edgar, D.M., Tricklebank, M.D., Wafford, K.A., and Jones, M.W. (2012). Decoupling of sleep-dependent cortical and hippocampal interactions in a neurodevelopmental model of schizophrenia. Neuron *76*, 526–533.

Prince, T.M., Wimmer, M., Choi, J., Havekes, R., Aton, S., and Abel, T. (2014). Sleep deprivation during a specific 3-hour time window post-training impairs hippocampal synaptic plasticity and memory. Neurobiol. Learn. Mem. *109*, 122–130.

Rasch, B., and Born, J. (2013). About sleep's role in memory. Physiol. Rev. *93*, 681–766.

Rosanova, M., and Ulrich, D. (2005). Pattern-specific associative long-term potentiation induced by a sleep spindle-related spike train. J. Neurosci. *25*, 9398–9405.

Rothschild, G., Eban, E., and Frank, L.M. (2017). A cortical-hippocampal-cortical loop of information processing during memory consolidation. Nat. Neurosci. *20*, 251–259.

Sarasso, S., Proserpio, P., Pigorini, A., Moroni, F., Ferrara, M., De Gennaro, L., De Carli, F., Lo Russo, G., Massimini, M., and Nobili, L. (2014). Hippocampal sleep spindles preceding neocortical sleep onset in humans. Neuroimage *86*, 425–432.

Schöne, C., Cao, Z.F., Apergis-Schoute, J., Adamantidis, A., Sakurai, T., and Burdakov, D. (2012). Optogenetic probing of fast glutamatergic transmission from hypocretin/orexin to histamine neurons in situ. J. Neurosci. *32*, 12437–12443.

Schreiner, T., Lehmann, M., and Rasch, B. (2015). Auditory feedback blocks memory benefits of cueing during sleep. Nat. Commun. *6*, 8729.

Sejnowski, T.J., and Destexhe, A. (2000). Why do we sleep? Brain Res. *886*, 208–223.

Siapas, A.G., and Wilson, M.A. (1998). Coordinated interactions between hippocampal ripples and cortical spindles during slow-wave sleep. Neuron *21*, 1123–1128.

Sirota, A., Csicsvari, J., Buhl, D., and Buzsáki, G. (2003). Communication between neocortex and hippocampus during sleep in rodents. Proc. Natl. Acad. Sci. USA *100*, 2065–2069.

Staresina, B.P., Bergmann, T.O., Bonnefond, M., van der Meij, R., Jensen, O., Deuker, L., Elger, C.E., Axmacher, N., and Fell, J. (2015). Hierarchical nesting of slow oscillations, spindles and ripples in the human hippocampus during sleep. Nat. Neurosci. *18*, 1679–1686.

Steriade, M. (2006). Grouping of brain rhythms in corticothalamic systems. Neuroscience *137*, 1087–1106.

Steriade, M., Domich, L., and Oakson, G. (1986). Reticularis thalami neurons revisited: activity changes during shifts in states of vigilance. J. Neurosci. *6*, 68–81.

Steriade, M., Nuñez, A., and Amzica, F. (1993). Intracellular analysis of relations between the slow (< 1 Hz) neocortical oscillation and other sleep rhythms of the electroencephalogram. J. Neurosci. *13*, 3266–3283.

Sullivan, D., Mizuseki, K., Sorgi, A., and Buzsáki, G. (2014). Comparison of sleep spindles and theta oscillations in the hippocampus. J. Neurosci. *34*, 662–674.

Tse, D., Langston, R.F., Kakeyama, M., Bethus, I., Spooner, P.A., Wood, E.R., Witter, M.P., and Morris, R.G.M. (2007). Schemas and memory consolidation. Science *316*, 76–82.

Tse, D., Takeuchi, T., Kakeyama, M., Kajii, Y., Okuno, H., Tohyama, C., Bito, H., and Morris, R.G.M. (2011). Schema-dependent gene activation and memory encoding in neocortex. Science *333*, 891–895.

Wang, D.V., Yau, H.J., Broker, C.J., Tsou, J.H., Bonci, A., and Ikemoto, S. (2015). Mesopontine median raphe regulates hippocampal ripple oscillation and memory consolidation. Nat. Neurosci. *18*, 728–735.

Wilson, M.A., and McNaughton, B.L. (1994). Reactivation of hippocampal ensemble memories during sleep. Science *265*, 676–679.

Xu, W., and Südhof, T.C. (2013). A neural circuit for memory specificity and generalization. Science *339*, 1290–1295.

Zhao, S., Ting, J.T., Atallah, H.E., Qiu, L., Tan, J., Gloss, B., Augustine, G.J., Deisseroth, K., Luo, M., Graybiel, A.M., and Feng, G. (2011). Cell type–specific channelrhodopsin-2 transgenic mice for optogenetic dissection of neural circuitry function. Nat. Methods *8*, 745–752.

STAR★METHODS

KEY RESOURCES TABLE

REAGENT or RESOURCE	SOURCE	IDENTIFIER
Antibodies		
Rabbit anti-PV antibody	Abcam	Abcam Cat# ab11427; RRID: AB_298032
Mouse anti-NeuN	Millipore	Millipore Cat# MAB377; RRID: AB_2298772
Alexa 555 goat anti-mouse IgG	Invitrogen	Molecular Probes Cat# A-21424 also A21424; RRID: AB_141780
Alexa 594 goat anti-rabbit IgG	Invitrogen	Molecular Probes Cat# A-11012 also A11012; RRID: AB_141359
VECTASHIELD HardSet Mounting Medium with DAPI antibody	Vector Laboratories	Vector Laboratories Cat# H-1500; RRID: AB_2336788
Bacterial and Virus Strains		
pAAV.CBA.flex.Arch-GFP.WPRE.SV40	Chow et al., 2010; UPenn Vector Core	Archaerhodopsin virus; AV-9-PV2432; Addgene 22222
pAAV.Ef1a.DIO.hCHR2(H134R)-EYFP.WPRE.hGH	Schöne et al., 2012; UPenn Vector Core	Channelrhodopsin virus; AV-9-20298P; Addgene 20298
pAAV.EF1a.DIO.EYFP.WPRE.hGH	Morel et al., 2014; UPenn Vector Core	YFP control virus; AV-9-27056; Addgene 27056
Deposited Data		
All Mice average Traces (FRO/PAR/CA1) – SO peak plot	This paper; Mendeley Data	http://dx.doi.org/10.17632/zpsnm54mvp.2
Experimental Models: Organisms/Strains		
*B6;SJL-Tg(Pvalb-COP4*H134R/EYFP)15Gfng/J; Prv-mhChR2-EYFP*	The Jackson Laboratory	RRID: IMSR_JAX:012355
129P2-Pvalb$^{tm1(cre)arbr}$ IJ; B6J PV-Cre	The Jackson Laboratory	RRID: IMSR_JAX:008069
Oligonucleotides		
Primer: Prv-mhChR2-EYFP, Forward: CTT TTC GCA CTT GCT CTG C	The Jackson Laboratory	N/A
Primer: B6J PV-Cre, Mutant Forward: GCG GTC TGG CAG TAA AAA CTA TC	The Jackson Laboratory	N/A
Software and Algorithms		
MATLAB	MathWorks	RRID: SCR_001622
Spike2	Cambridge Electronic Design (CED)	RRID: SCR_000903
Statistical Package for Social Sciences (SPSS)	IBM	RRID: SCR_002865
FreeFrame	Coulborne	RRID: SCR_014429
EthoVision XT	Noldus	RRID: SCR_000441
Online closed-loop detection of slow oscillation and stimulation trigger	This paper; Mendeley Data	http://dx.doi.org/10.17632/c872f83pdz.4
Offline sleep staging	This paper; Mendeley Data	http://dx.doi.org/10.17632/c872f83pdz.4
Slow oscillation detection algorithm	Ngo et al., 2013; Mendeley Data	http://dx.doi.org/10.17632/c872f83pdz.4
Spindle detection algorithm	Gardner et al., 2013 (spindle detection algorithm); Mendeley Data	http://dx.doi.org/10.17632/c872f83pdz.4
Ripple detection algorithm	Rothschild et al., 2017 (ripple detection); Mendeley Data	http://dx.doi.org/10.17632/c872f83pdz.4

CONTACT FOR REAGENT AND RESOURCE SHARING

Further information and requests for resources and reagents should be directed to and will be fulfilled by the lead contact, Hee-Sup Shin (shin@ibs.sre.kr).

EXPERIMENTAL MODEL AND SUBJECT DETAILS

Mice

Prv-mhChR2-EYFP (tg/+) transgenic mice (RRID: IMSR_JAX:012355), maintained in a C57BL/6J background (B6j), were used for the main behavior experiment (Figure 1E: Fear Conditioning behavior, n = 26; Electrophysiology, n = 29; see table below for details). The same transgenic mice were used for the complementary behavior experiment, object place recognition task (Figure S1: Object Place Recognition, n = 26; see below table for details). Prv-cre knockin mice (RRID: IMSR_JAX:008069; B6; 129P2-Pvalb$^{tm1(cre)arbr}$ IJ) were used for the virus-mediated inhibition experiment (Archaerhodopsin; Fear Conditioning behavior, n = 24; see below table for details) and for the virus-mediated control for alternative stimulation protocols (GFP/Channelrhodopsin; Fear Conditioning behavior, n = 24; Electrophysiology, n = 21; see table below for details). An additional set of mice were used to test the effect of an non-spindle-like stimulation (20Hz, 5msec pulse, total duration: 0.5 s, timing: in-phase) on TRN activity on fear conditioning behavior (Behavior, n = 17; Electrophysiology, n = 17; see Table S4 for detail). All mice were generated using an in vitro fertilization method employing foster ICR female mice (male sperm: B6j Prv-mhChR2-EYFP (tg/+), female: wild-type B6j) or in mating cages (B6j Prv-cre (cre/+) male back-crossed with wild-type B6j females). Mice were maintained under a 12 hr light/12 hr dark cycle (light cycle beginning at 8:00 a.m.), and were provided free access to food and water. Male mice only were used at 11–14 weeks of age and housed in pairs with a transparent acrylic partition (one animal per side to preserve recording connectors and optic fiber cannulas). Animal care was provided and all experiments were conducted in accordance with the ethical guidelines of the Institutional Animal Care and Use Committee of the University of KAIST (site of the experiment) and the Institute for Basic Science, Korea.

METHOD DETAILS

Surgery

Surgical implantation of optic fiber cannulas and electrodes for recordings of EEGs, EMGs, and LFPs was performed under ketamine/xylazine anesthesia (20 ml/kg, i.p.). Following administration of the anesthetic, mice were restrained in a stereotaxic device (David Kopf Instruments, USA). All the following stereotaxic coordinates are given with reference to the bregma (Paxinos and Franklin, 2004) as anterior-posterior (AP), medial-lateral (ML) and, when applicable, dorsal-ventral (DV). For EEG recordings, two stainless steel screws were fixed to the skull over the right PFC (AP: +1.48 mm; +ML: 0.3 mm) or the right PAR (AP: −4.03 mm: +ML, 1.5 mm). An additional screw was positioned above the cerebellum region and used as a reference. An uncoated stainless steel wire (inner diameter, 76.2 μm; A-M Systems, USA) was tied to the nuchal muscle for EMG recordings. For LFP recordings, a formvar-insulated nichrome wire (inner diameter, 50.8 μm; impedance, 400 kΩ; A-M Systems) was implanted into the right CA1 region of the hippocampus (AP: −2.03 mm; ML: +1.1 mm; DV: +1.2 mm). All wires were attached to a custom-made electronic interface board with an 18-pin connector (Omnetics, USA). Monofiber optic cannulas (inner/outer diameter, 100/125-0.22; length, 4 mm; ZF1.25 DFL; Doric Lens, Canada) for performing optogenetic stimulation were implanted bilaterally in the rostral-ventral region of the TRN (AP, −0.6 mm; ML, +/−1.5 mm; DV, 3.2 mm; incline, 20 degrees). Prv-cre mice received bilateral injection (0.5 uL on each side) of pAAV.CBA.Flex.Arch-GFP.WPRE.SV40 (addgen 22222, Upenn) for the archaerhodopsin mediated inhibtion. For the control experiment based on a non-spindle-like stimulation, pAAV.EF1a.DIO.EYFP.WPRE.hGH (addgen: 27056, Upenn) and pAAV-EF1a-DIO-hCHR2(H134R)-EYFP.WPRE.hGH (addgen: 20298, Upenn) viruses were used, respectively. All mice were housed by two with a transparent acrylic partition in order to preserve the optic fiber and electronic interface board (EIB) from grooming behavior. All mice were allowed 5 days (Prv-mhCHR2-EYFP, surgical implantation) or 3 weeks (Prv-cre; surgical implantation and viral expression) to recover following surgery before proceeding with the experiment.

Histology

Following anesthesia with 0.2% tribromoethanol (20 ml/kg, i.p.), mice were first perfused with saline (0.9%) and then with a 4% paraformaldehyde solution (100 mL). Their brains were then removed and cut into 50-μm-thick coronal sections with a vibratome (Leica, Germany). For immune staining (Figures 6B and 6D), brain sections are washed three times in PBS and blocked in PBS containing 0.5% Triton X-100 and 5% normal goat serum Sections are then incubated for ∼16 hr at room temperature in rabbit anti PV antibody (1:500, ab11427, Abcam; RRID: AB_298032), mouse anti-NeuN (1:2000, MAB377, Millipore; RRID: AB_2298772). Following incubation, sections are washed three times in PBS and then incubated for 2 hr at room temperature in Alexa Fluor 555 goat anti-mouse IgG (1:500, Invitrogen; A21424 RRID: AB_141780), Alexa Fluor 594 goat anti-rabbit IgG (1:500, Invitrogen; A11012 RRID: AB_141359), are then washed three times in PBS and followed by three 10 min rinses in PB and mounted on glass slides with Hardset Vectashield (Vector Labs; H-1500 RRID: AB_2336788) for microscopy. Photographs were taken using either an Eclipse-Ti microscope (Nikon, Japan) or a FluoView FV1000 confocal laser-scanning system (Olympus, Japan). Histological results summarized in Figure S1 show the bilateral positioning of fiber optic cannula as well as fluorescence detection of channelrhodopsin expression and a representative recording site in the CA1 hippocampal region.

Procedure and Design

After full recovery from surgery, all mice were handled daily for 15 min on five consecutive days to habituate them to the human experimenter. On the fifth day, an open field test was performed for 30 min in a quadratic recording box (40 × 40 × 40 cm) constructed of

acrylic white polyvinyl chloride; mice were subject to continuous video surveillance to identify and exclude mice with abnormal locomotion (Ethovision XT, Noldus, USA; RRID: SCR_000441; 2 mice). The open field box was positioned in a soundproof and light-intensity, temperature- and humidity-controlled behavior chamber (cantered LED light, 4 lux; temperature, 22°C; humidity, 60%) with ambient white noise (80 dB) and two fans for air circulation. On the following day, the mice, located inside a sleep chamber equipped with a fan and light, and in the presence of 80-dB ambient white noise, were acclimated to the attachment of connectors for signal recording and photostimulation devices for 6 hr (no stimulation was given). On experimental days (Figure 1, main text), mice were acclimated to the behavior chamber in the presence of white noise for 30 min. Conditioning of the contextual fear-conditioning commenced at 8:30 a.m. Based on previous work demonstrating a critical window for memory consolidation in the first few hours after encoding (Boyce et al., 2016; Graves et al., 2003; Prince et al., 2014) the mice were immediately placed into the sleep recording box (~9:00 a.m.) for 6 hr, during which they received stimulation when NREM slow oscillations were detected. After this 6-h stimulation period, all mice were returned to their home cage for another 18 hr. The following day, the test phase of the learning task—24h memory recall—began at 8:30 a.m., preceded by the same acclimation procedure described above. Prv-mhChR2-EYFP mice and Prv-cre mice were randomly assigned to their stimulation groups following the fear conditioning task (FC) and object place recognition task (OPR). The table below shows the number of mice for behavioral tests and electrophysiological recordings used in the FC and OPR experiments, for each mouse line and corresponding viral injection. Numbers of mice with both behavioral and 33 electrophysiological recordings are indicated in brackets. EEG data are for both FRO and PAR leads.

	NoSTIM	IN	OUT	Total
Prv-mhChR2-EYFP				
FC				
Behavior	10 (10)	8 (6)	8 (8)	26 (24)
EEG	11	9	9	29
CA1	9	8	8	25
OPR				
Behavior	11	8	7	26
EEG	9	8	7	24
CA1	9	8	6	23
Prv-cre × DIO-ARCH				
FC				
Behavior	9 (7)	8 (8)	7 (5)	24 (20)
EEG	8	8	5	21
CA1	7	8	5	20

Contextual Fear Conditioning

To simultaneously assess effects of spindle stimulation on aspects of memory that do and do not essentially rely on hippocampal function, we used a combined cue/contextual fear-conditioning paradigm (adapted from Boyce et al., 2016; Figure 1, main text). During the conditioning phase, mice were placed in a metallic rectangular chamber with a surface grid (context A) connected to an electrical shocker (Coulbourn Instruments, USA). Mice were habituated to the box for 3 min followed by application of two successive tone-shock pairs separated by an interval of 2 min. Each tone (2 kHz at 85 dB) lasted for 30 s and was accompanied by a foot shock (0.75 mA, 5V) that occurred during the last 2 s. On the following morning, 24 hr contextual fear memory was first tested by placing the mouse in the same context A as during conditioning for 8 min. Then, after a 3 hr break, cued (tone) fear recall was tested in a different context B. For this, the mouse was placed in a black, round acrylic cylinder (diameter, 30 cm) with wood bedding for 3 min followed by a single presentation of the tone for 30 s. Contextual fear memory was determined (per minute) based on the freezing behavior displayed by the mouse, averaged across the first 4 min. Cued fear to the tone presentation was determined by the relative amount of freezing during the 1 min interval following tone onset. Freezing behavior during conditioning were assessed blindly to the experimenter using an automatic freezing counter (FreezeFrame, Coulborn Instruments, USA; RRID: SCR_014429) and averaged across the last 1 min interval. The freezing during last minute of condition showed comparable values among the three stimulation conditions for the Prv-mhChR2-EYFP mice (Fear Conditioning; $F_{2,23} = 0.681$, $p = 0.516$, one-way ANOVA) and the Prv-cre mice (Fear Conditioning, inhibition experiment; $F_{2,23} = 0.060$, $p = 0.942$, one-way ANOVA).

Object Place Recognition Task

Prv-mhChR2-EYFP mice (n = 26) were given a 3 × 6 min for the exploration of an open-box (identical to the open field box: acrylic white, 40 × 40 × 40 cm) where two identical objects (toy soft sphere of 15 cm diameter) were positioned parallel to the box wall

(sampling period). For each mouse, the initial position of the objects was positioned randomly (parallel to one of the four walls) to avoid any side effect. Following this training, mice were assigned to their stimulation groups and placed in the sleep box for a period of 6hours. At the end of the stimulation period, mice were returned to their home cage within the mouse facility. The 24 hr test consisted of a single 6 min-exploration of the same identical objects with one at its original position (static object) and one having been displaced at an opposite corner (displaced object) in the open field box. The 24 hr delta preference is the change in preference toward the displaced object and is estimated as the difference in percentage preference for the displaced object at the last sampling period (last 6 min) and the test period (24 hr recall, 6 min). The object exploration behavior was quantified from video scoring from two independent researchers assigned blindly to the scoring of each video (sampling and testing videos).

Electrophysiological Recordings and Closed-Loop Optogenetic Stimulation Setup

EEG, EMG, and LFP recordings were digitized at 16 kHz using a Digital Lynx DX64 A/D converter and a Neuralynx 16-Channel analog headstage amplifier (HS-16; unity gain and hardware amplification gain = 10; Neuralynx, USA). Signal acquisition and recordings were performed using Cheetah software (version 5.6.3; Neuralynx, USA). Bandpass filters used were 0.1-45 Hz for EEG, 70–250 Hz for EMG. For CA1 LFP, broadband (0.1-7000Hz) and bandpass filtered signal (100–250 Hz) were recorded. Signals were stored on a personal computer with a sampling frequency of 1 kHz for offline analysis. For the online detection of slow oscillations, the frontal EEG signal was acquired via the analog output and low-pass filtered with a custom-made 4-pole Butterworth filter (cut-off at 3 dB, 6 Hz). The filtered signal was fed, together with a bandpass-filtered EMG signal (using Neuralynx Cheetah software; cut-offs, 7 and 250 Hz) to the analog input of an Arduino UNO board (sampling rate, 80 Hz; Arduino LLC, https://www.arduino.cc/). A custom-made MATLAB code (Mathworks, USA; RRID: SCR_001622) provided online-monitoring of the current sleep stage to ensure stimulation during NREM sleep and automatic detection of slow oscillations using an adaptive thresholding method (Ngo et al., 2013, 2015) to control optogenetic stimulation. The semi-automated online sleep stage monitoring was used to provide a stand-by signal to the slow oscillation detection method and was combined with the low-pass filtered FRO EEG signal (0.1–6 Hz) and the band-pass filtered EMG signal (70–250 Hz); the latter was then rectified and integrated over 3 s to provide an index of muscle tone. Wakefulness was identified for a combination of filtered FRO EEG lower $Th_{EEG\text{-}wake}$ (static threshold: three times the standard deviation of the last 10sec activity) and muscle tone in the EMG higher than $Th_{EMG\text{-}wake}$ (static threshold: 50 percent of the maximum value of EMG index, out of all past value acquired). Rapid eye movement (REM) sleep showing a dominant 6–8 Hz in EEG was characterize by a filtered FRO EEG lower than $Th_{EEG\text{-}wake}$ (i.e., same threshold as for wake) and EMG index lower than $Th_{EMG\text{-}REM}$ (static threshold: 20 percent of the maximum value of EMG index, out of all past value acquired). The identification of WAKE stage resulted in a 10 s on-going deactivation of the slow oscillation detection system. REM stage had intrinsically no slow oscillation or high amplitude event and could not trigger the slow oscillation detection. The rate of erroneous stimulations (i.e., those not occurring in NREM sleep) was always < 7%, and mainly resulted from delayed identification of a change in sleep state (i.e., mostly REM to WAKE). NREM sleep was defined as a non-WAKE/non-REM and showed EMG index value lower then $Th_{EMG\text{-}wake}$ and higher propensity for slow oscillations (< 4Hz; i.e., FRO EEG higher than $Th_{EEG\text{-}wake}$). Once identified, NREM sleep enabled activation of the slow oscillation detection algorithm. EEG and EMG power criteria for classifying sleep stages were individually adjusted based on offline scored sleep recordings of the respective animal, obtained prior to the experiment.

Slow oscillations were detected by subjecting the filtered frontal EEG signal to an amplitude-based threshold criterion. Whenever the signal crossed the threshold (default value, −3.5 mV, after 10-fold hardware amplification from the unit-gain acquisition) from above toward more negative values, a stimulus was triggered. To adapt for fluctuations in the negative peak amplitude of the slow oscillation, we re-set the threshold every 0.5 s to the largest minimum within the last 5 s, if this minimum value was also smaller than the default value. During in-phase stimulation, upon each detection of a slow oscillation negative half-wave, the Arduino board sent a TTL signal to a Master-8 signal generator (A.M.P.I., Israel), which triggered a 4-cycle square wave with on/off periods of 62.5 ms (corresponding to 8 Hz) or a continuous pulse of 500msec duration (optic inhibition using archaerhodopsin in Prv-cre mice). The total response delay of the system, resulting from (i) the Arduino-to-MATLAB acquisition (UBS 2.0; 20 ms), the detection algorithm (50 ms) and the emission of a digital output (USB 2.0; 20 ms), amounted to 90 ms. The on/off spindle-like sequence was used to drive the output from a DL-445-050-O blue-light laser with a wavelength of 445 nm (CrystalLaser, USA), which propagated via an optical patch cord to the connected optical fibers in the mouse TRN. For optogenetic inhibition, we used a continuous pulse of 500msec duration from a MGL-FN-561 yellow-light laser with a wavelength of 561nm (CNI Optoelectronics Technology Co. Ltd., China). Stimulation started (with a 90-ms delay after detection of a negative half-wave peak) at about the late transition into the depolarizing up-state. A stimulation frequency of 8 Hz (four light-pulses, 62.5 ms on/off duration) was chosen based on previous work demonstrating a reliable induction of sleep spindles with this protocol (Kim et al., 2012) as it corresponds to the predominant firing pattern at approximately 8-Hz observed in the TRN during spontaneous (Contreras and Steriade, 1996; Steriade et al., 1986). During out-of-phase stimulation, the stimulus onset commenced randomly between 0.7 and 1.2 s after detections, ensuring stimulation in the absence of a slow oscillation. In the no-stimulation control protocol, the procedure was identical to the in-phase condition except that no optogenetic stimulus was applied. The laser output was calibrated to 4 mW at the end of the optical fiber cannula before each experiment using a PM100D power meter (Thorlabs, USA). Post hoc visual inspection of

the stimulation by two independent experimenters revealed an accuracy of > 86%. The number of stimuli delivered during NREM sleep was comparable among all conditions (in-phase = 535.7, out-of-phase = 678.4 and no-stimulation = 594.5455; $F_{2,26} = 1.399$ and $p = 0.265$, one-way ANOVA).

QUANTIFICATION AND STATISTICAL ANALYSIS

Analyses of Sleep Measures and EEG

All analyses were performed using MATLAB and Spike2 software (Cambridge Electronic Design, UK; RRID: SCR_000903) based on custom-made scripts. EEG and EMG signals during the 6 hr recording periods were visually scored by two experienced raters into 10 s epochs of NREM, REM sleep, and wake intervals. Epochs with artifacts or movement arousals were visually identified and excluded from further analysis. Total sleep time, first onset of NREM sleep, and time spent in the different sleep stages were then determined for the total intervention interval.

Evoked Potentials

Immediate effects of optogenetic stimulation were analyzed by averaging EEG and LFP signals, time-locked to stimulation onsets, within a 1.5 s window starting 0.5 s prior to the onset of a spindle-like stimulation. Both prefrontal and parietal EEG signals were band-pass-filtered at 0.3–30 Hz, 0.5–4 Hz, and 7–10 Hz to allow inspection of the broad sleep EEG signal, slow oscillatory activity, and spindle activity, respectively. Filtering in the slow oscillatory and spindle bands was followed by a root mean square (RMS) calculation and smoothing using a moving average based on a 200-ms window and a step size of 10 ms, yielding transient power measures within the respective frequency bands.

Offline Detection of Sleep Spindles, Ripples, and Slow Oscillations

Discrete spindles and ripples were detected using offline algorithms adopted from references (Gardner et al., 2013; Rothschild et al., 2017), respectively. For spindle detection, the EEG signal was bandpass-filtered at 7–10 Hz and the envelope determined using the Hilbert transform. Please note, the lower spindle range was chosen to accentuate the 8-Hz spindle stimulation protocol. However, for all analysis a spindle detection based on a frequency range from 7-15 Hz revealed identical results. A potential spindle event was identified in cases where the envelope exceeded an individual threshold defined by the standard deviation of the envelope across all NREM sleep epochs, multiplied by 3.5. Onset and end of potential spindle events were marked by the crossing of a second lower threshold at 2 times of the standard deviation of the envelope. Subsequently, potential spindle events with durations shorter than 0.4 or longer than 3 s were discarded. For ripple detection, the LFP signal was likewise filtered at 100–250 Hz and the envelope determined. A ripple event was identified in cases where the envelope exceeded an individual threshold which was defined by the standard deviation of the envelope across all NREM sleep epochs, multiplied by 5.0. Onset and end of potential ripple events were marked by the crossing of a second lower threshold at 2 times of the standard deviation of the envelope. Then, the respective event was discarded if it was shorter than 40 ms or longer than 500 ms. For subsequent analysis the remaining ripple events were marked by their most negative peak. Visual inspection of the offline detected spindle and ripple events by two experiences raters revealed an accuracy of > 95%.

The efficacy of stimulation in inducing spindle and ripple events was examined by calculating the sum of discrete events overlapping with a 0–0.75 s window post-stimulation onset, then dividing it by the total number of spindle-like stimulations and multiplying it by 100 to yield percentages. Time-event correlation histograms were then calculated for spindle troughs (i.e., the minima of the filtered signal within each spindle interval), which were time-locked to the onsets of the spindle-like stimulation, covered a 1.25 s window starting 0.5 s prior to stimulation onset, and had a bin size of 0.01 s. The grouping of ripples by spindles was assessed by calculating event-correlation histograms for ripple events (with an event indicated by the most negative peak of the ripple), that were phase-locked to the spindle troughs and covered a 1 s window with an offset of 0.5 s and a bin size of 0.01 s.

Discrete slow-oscillation events during NREM sleep were detected following previously described procedures (David et al., 2013; Mölle et al., 2009). In brief, the EEG was bandpass-filtered at 0.2–4.5 Hz and, then all positive-to-negative zero crossings of the signal, as well as the local minimum and maximum between each two successive crossings, were marked. Intervals between two successive zero-crossings were identified as a slow-oscillation event in cases where the length of this interval was between 0.4 and 2 s (corresponding to 0.5 to 2.5Hz) and the minimum amplitude and minimum-to-maximum amplitude ratio were greater than 66.6% of the average of the respective amplitude values across the whole recording epoch.

Statistical Analysis

Unless stated otherwise, data are graphically presented as box-whisker-plot and numerically as means ± SEM. Statistical analyses were performed using SPSS version 23 (IBM, USA; RRID: SCR_002865). All data were initially examined for normality using a Kolmogorov-Smirnov test. For most analyses, a parametric one-way analysis of variance (ANOVA) or Kruskal-Wallis test was performed. The main group factor was "stimulation condition" (Prv-mhCHR2-EYFP: IN, OUT and NoSTIM, or when appropriate, IN, OUT, NoSTIM-IN and NoSTIM-OUT; Prv-cre: IN-ARCH, OUT-ARCH, NoSTIM). Post hoc analyses to a significant ANOVA result were performed for independent samples using Fisher's least significant difference (LSD) t test approach, with correction for family-wise error or, depending on the equality of variance and normality, a Welch- or Ranksum test. All statistical analysis performed

in the main text are summarized in detail in Table S5. No power analysis was performed prior to the experiments. However, sample size for each group was matched to numbers typically used in comparable rodent studies.

DATA AND SOFTWARE AVAILABILITY

All data including behavior video files (Fear Conditioning: FreezeFrame, RRID: SCR_014429; Open-field and Object place recognition task: Ethovision XT, RRID: SCR_000441), raw recording files (Neuralynx .csc files), real-time analysis codes (MATLAB m-files), figure generation code (Spike2: RRID: SCR_000903/MATLAB: RRID: SCR_001622) and demonstration video are available on demand by email at the address: charles@ibs.re.kr or referenced in the STAR Methods Key Resources Table.

Neuron, Volume *95*

Supplemental Information

Thalamic Spindles Promote Memory Formation during Sleep through Triple Phase-Locking of Cortical, Thalamic, and Hippocampal Rhythms

Charles-Francois V. Latchoumane, Hong-Viet V. Ngo, Jan Born, and Hee-Sup Shin

Supplementary Data

Figures S1-S7

Table S1-S4

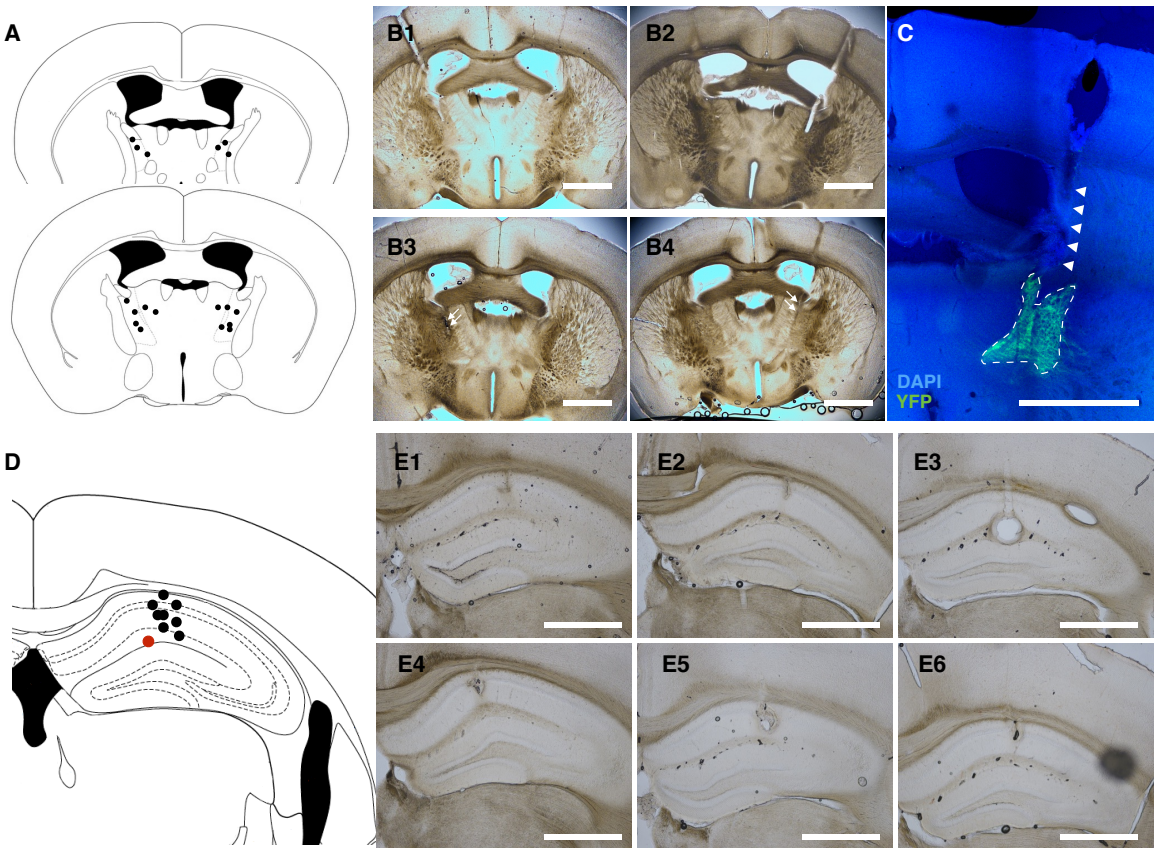

Supplementary Figure 1. **Histological verification of optical fiber location and LFP recording site. Related to Figure 1.**

(**A**) Schematic coronal sections (AP: -0.46 and -0.58) indicating the location of the end tip of implanted fiber optic cannulae for the in-phase group of the main experiment (n = 9).

(B) Left (B1 and B3) and right (B2 and B4) optic fiber tracks for two representative mice under a bright field. White arrows mark the position of the fiber track for the second mouse. The white scale bar represents 1 mm.

(**C**) Representative fluorescence image of mhChR2-eYFP within the TRN of one transgenic mouse tested in the main experiment; white triangles indicate the fiber optic track and the dashed lines delineated the TRN boundary. YFP expression is overlaid on a DAPI staining. Scale bar represents 1 mm.

(D) Schematic coronal section (AP: -2.06) illustrating the positioning of the hippocampal LFP electrode for the in-phase group in the main experiment (n = 9). The red dot indicates a mouse

that has been discarded due to a bad electrode positioning and signal quality. Note, most recordings are localized within the stratum radiatum or pyramidale.

(E) Histology of six representative mice showing the electrode tracks and lesion sites corresponding to the location where hippocampal LFP was recorded. Scale bar represents 1 mm.

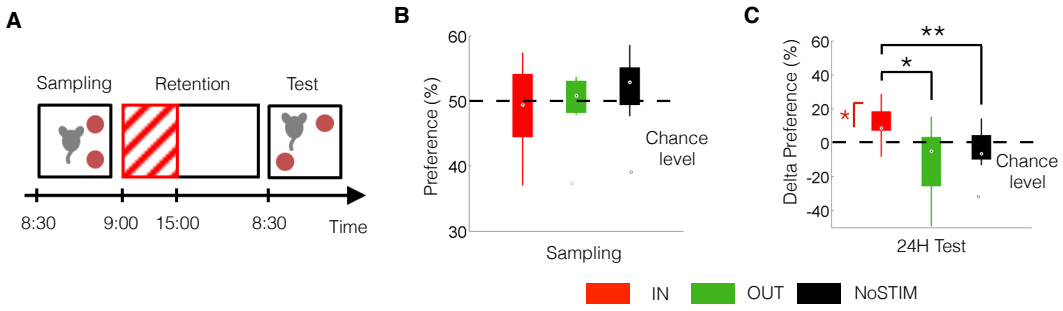

Supplementary Figure 2. In-phase spindle-like stimulation enhanced spatial memory in an object place recognition task. Related to Figure 1.

(A) Experimental design to assess effects on spatial memory with a hippocampal dependent object place recognition task in Prv-mhChR2-eYFP mice (n = 26). Following a sampling phase, the animals were allowed to sleep and were subjected to one of three stimulation protocols for 6 hours (red hatched area). Spatial memory was tested the next morning 24 hours after the learning phase. Please see Methods for further information on the object place recognition task.

(B) Preference during the Sampling phase for the displaced object calculated as the percentage of time spent exploring the displaced object over the total time spent exploring both objects. A 50% preference represents no preference for either of the objects; Analysis of learning performance assured that exploratory preference behavior was comparable between the in-phase (IN, red), out-of-phase (OUT, green) and no-stimulation condition (NoSTIM, black) during the last sampling phase before sleep (Kruskal-Wallis one-way ANOVA, $U_2 = 1.752$, $P = 0.416$).

(C) Object place recognition memory at recall test after in-phase (IN, red), out-of-phase (OUT, green) and no-stimulation (NoSTIM, black). ** $P < 0.01$, * $P < 0.05$, for post-hoc pairwise comparisons. All data is presented as a box-whisker plots, in which the white dot represents the median, box limits the first and third quartile and the whiskers represent the minimum and

maximum values of the raw data; one-way ANOVA, $F_{2,23} = 4.374$, $P = 0.025$, NoSTIM vs IN $P = 0.042$, NoSTIM vs OUT $P = 0.333$, IN vs OUT $P = 0.009$. $^{**}P < 0.01$, $^{*}P < 0.05$, Fisher LSD for post-hoc pairwise comparisons. Following in-phase stimulation spatial memory was also significantly above chance level as indicated by the red asterisk (reference value: 0; one sample test, bootstrapping 1000 samples; $t_7 = 2.893$, $P = 0.023$).

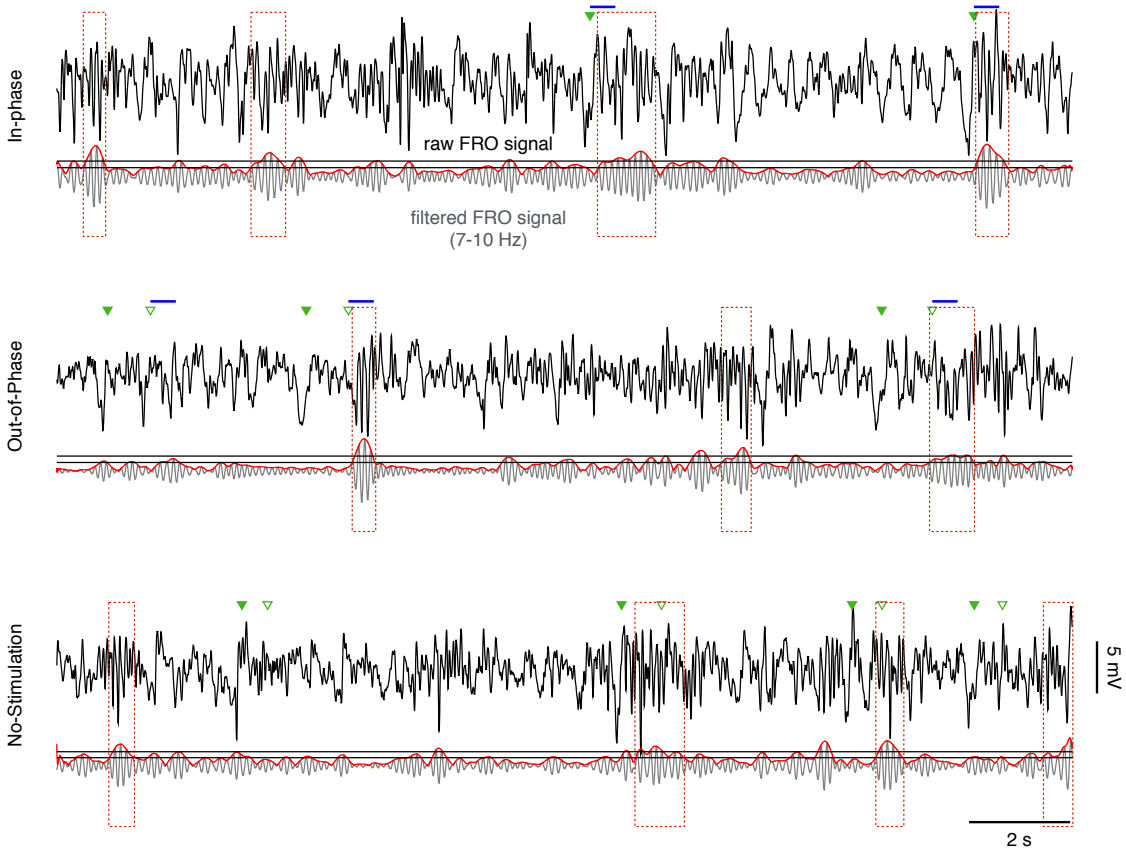

Supplementary Figure 3. **Representative traces illustrating the stimulation protocols. Related to Figure 2.**

20-second long traces of raw frontal (FRO) EEG recordings (black lines), filtered in the 7-10 Hz spindle band (grey lines underneath), envelop from Hilbert transform (redlines) and spindle detection thresholds (horizontal black lines for lower and higher threshold), for the in-phase (top), out-of-phase (middle) and no-stimulation condition (bottom). Blue bars indicate 500-ms intervals comprising light stimulation commencing with the up-state of a detected slow oscillation during in-Phase stimulation (filled green triangle) or with a random delay between 0.5 to 1.0 s (empty green triangle) during out-of-phase conditions. In the no-stimulation condition intervals serving as control for the in-phase and out-of-phase conditions are indicated by filled green and empty green triangles, respectively. Offline identified discrete spindle events are framed by dashed squares. The horizontal black lines overlaid on

the filtered signal indicate the two individually determined threshold used to identify the discrete spindle events.

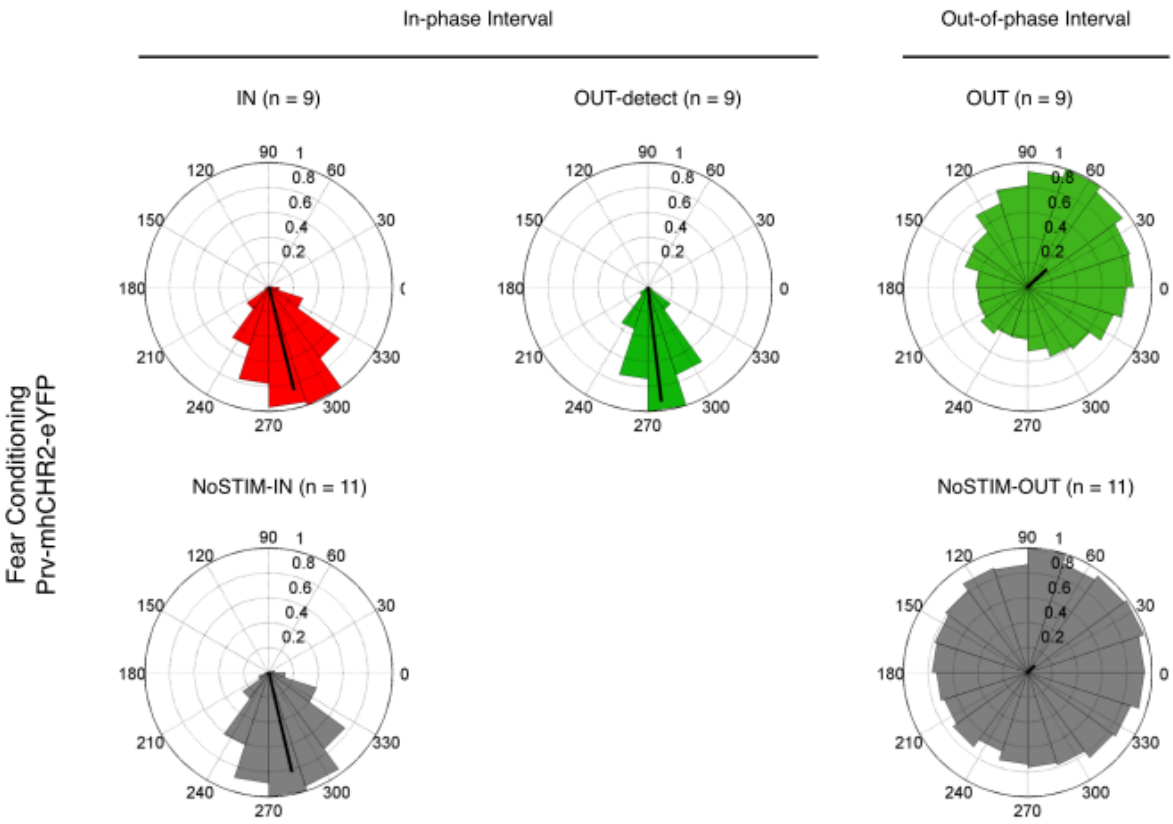

Supplementary Figure 4. Phase plots showing stimulation onset for the different stimulation protocols. Related to Figure 2.

Phase preference of stimulation onset in the in-phase (IN), out-of-phase (OUT) stimulation conditions and in respective control conditions (No stimulation group: NoSTIM-IN, NoSTIM-OUT; OUT following a detection: OUT-detect) during NREM sleep following fear conditioning. Phase angles were estimated from the bandpass filtered (0.3 - 4.5 Hz) EEG. Zero degrees refers to the up-to-down zero crossing of the wave. The black line within each circular histogram plot represents the mean angular vector. Note, whereas in-phase stimulation (IN mean phase/kappa: 283.8°/3.69), as well as respective marks in the NoSTIM-IN (mean phase/kappa: 283.1°/3.15) and OUT-detect (mean phase/kappa: 276.8°/7.05) conditions, consistently occurred around 270°, corresponding to a slow oscillation up-state emerging after an identified down-state (i.e., negative slow oscillation half-wave peak), no consistent phase relation is observed during out-of-phase conditions (OUT: mean

phase/kappa: 42.8°/0.43; NoSTIM-OUT: mean phase/kappa: 43.1°/0.16; Watson-William multi-sample test for equality of mean angle, $F_4 = 2400$, $P < 0.001$) . Also, it is to note in this context that, with regard to the reoccurrence of a down-state (following the detected down-state) the slow oscillation does not represent a sine-wave like oscillation as the duration of the up-state is highly variable.

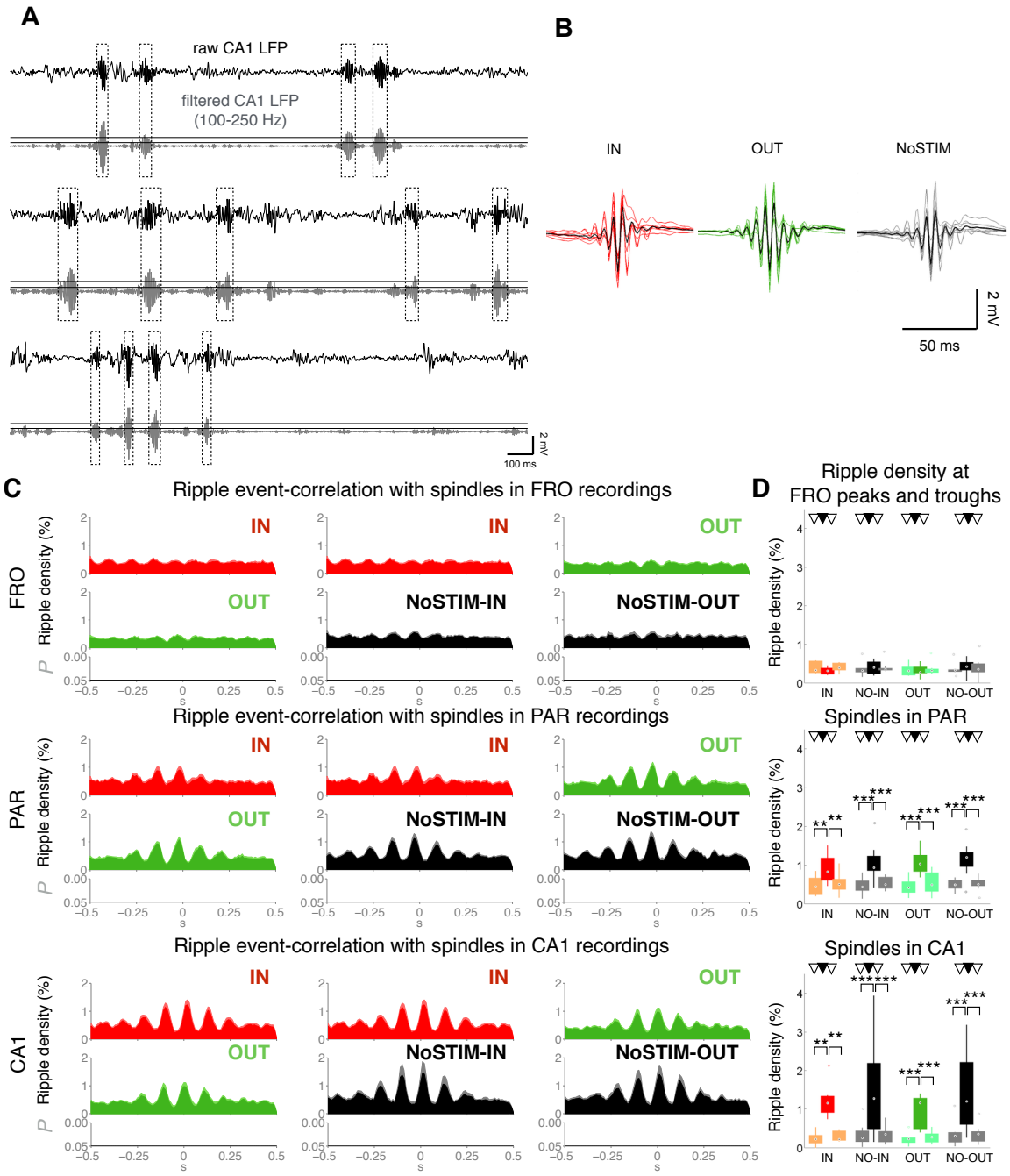

Supplementary Figure 5. Ripple detection and event-correlation histograms show grouping of hippocampal ripples phase-locked to PAR and CA1 spindles. Related to Figure 5.

(A) Three 2.5-s long examples showing the raw and band pass filtered (150-250 Hz) hippocampal LFP signal with offline detected ripples events marked by the dashed squares. The horizontal black lines indicate the two threshold used for the detection of these events.

(B) Average ripples detected for IN, OUT and NoSTIM groups. Thin lines represent averaged ripples for individual mice and thick black line indicate group average. Averaging was performed time-locked to the maximum negative peak of identified ripples.

(C) Mean ± SEM event-correlation histogram (across mice) of ripple events in LFP recordings from CA1 indicating that ripple density increased time-locked to spindle-troughs identified in FRO, PAR and CA1 recordings. Ripple density % refers to the number of detected ripple events (as marked by their most negative peak) per 10-ms bin divided by the number of stimulations during the 6-h intervention, multiplied by 100). Left column: Comparison between in-phase (IN: red histogram) and out-of-phase stimulation (OUT: green histogram). Middle and right columns: Comparison of in-phase or out-of-phase stimulation with corresponding periods of the no-stimulation conditions, NoSTIM-IN and NoSTIM-OUT (black histograms), respectively.

(D) Mean ± SEM number of CA1 ripple events occurring during the spindle troughs (filled black triangle) and peaks (empty black triangles) in FRO, PAR and CA1 recordings during in-phase (red) and out-of-phase stimulation (green) and no-stimulation period, NoSTIM-IN (hatched red) and NoSTIM-OUT (hatched green), respectively. *** $P < 0.001$, ** $P < 0.01$, for post-hoc pairwise comparisons. Note: The temporal distribution of ripple events did not consistently differ between stimulation conditions.

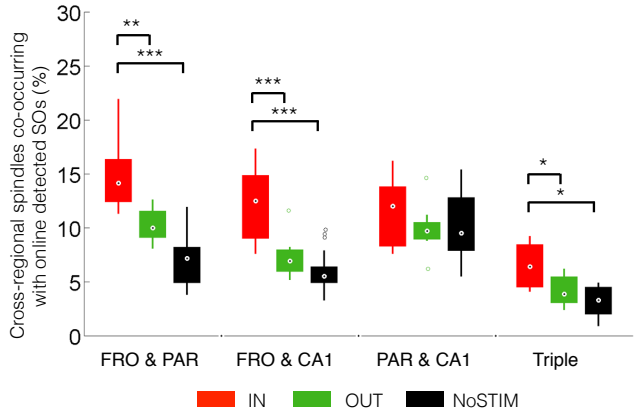

Supplementary Figure 6. In-phase stimulation increases the cross-regional co-occurrence of spindles. Related to Figure 5.

Incidence rate (in percent of total number of stimulations) of offline detected spindle events co-occurring in frontal and parietal (FRO & PAR), frontal and hippocampal (FRO & CA1), parietal and hippocampal (PAR & CA1) or all three recording sites (triple) following stimulation onset during in-phase (IN, red), out-of-phase (OUT, green) and no-stimulation conditions (NoSTIM, black). ***P < 0.001, ** P < 0.01, *P < 0.05, for post-hoc pairwise comparisons; data is shown as box-whisker-plots with box limits representing the first and third quartile and whiskers indicating the data range.

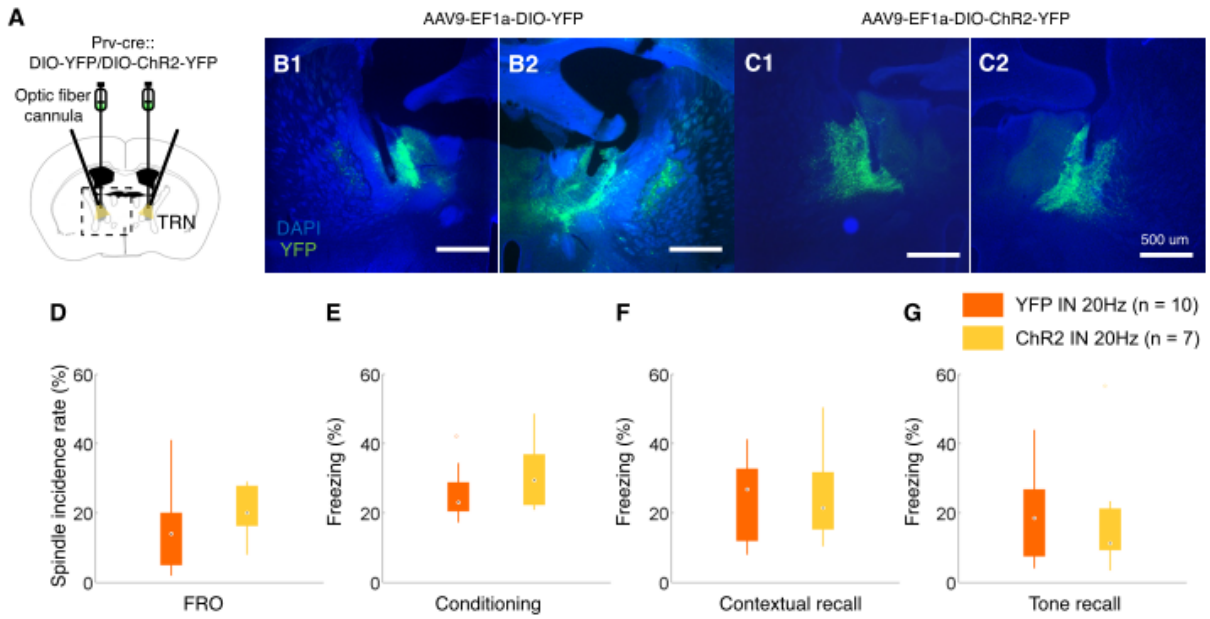

Supplementary Figure 7. TRN stimulation at a non-spindle frequency (20 Hz, duration 500 ms) in-phase with the SO upstate did not affect memory or spindle incidence. Related to Figure 6.

(A) Viral injection was performed and followed by fiber optic cannula implantation targeting the TRN bilaterally.

(B) Representative optic fiber position and YFP expression following the injection of pAAV-DIO-YFP in the left (B1) and right TRN (B2).

(C) Representative optic fiber position and YFP expression following the injection of pAAV-DIO-ChR2-YFP in the left (C1) and right TRN (C2).

(D) Spindle incidence rate (in percentage of given stimulation) derived from a 750-ms interval following stimulation onset. No statistical differences were found for spindle incidence (FRO: $F_{1,15} = 1.361$, $P = 0.262$).

(E) Percentage of freezing per min at the last minute of fear conditioning (see Methods for task procedure).

(F) Average freezing (percentage per min) of the first 4 minutes during contextual recall, 24 hours after conditioning.

(G) Freezing to the conditioned cue/tone in a different context 24-h after conditioning. Note: no statistical differences were found during conditioning of freezing ($F_{1,15} = 1.365$, $P = 0.261$), at contextual recall ($F_{1,15} = 0.017$, $P = 0.899$) and tone recall ($F_{1,15} = 0.021$, $P = 0.886$) between the YFP and ChR2 groups.

Supplementary Table 1. Sleep architecture for the Prv-mhChR2-eYFP transgenic mice during the 6 hours of spindle-like stimulation following fear conditioning. Related to Figure 1.

	In-phase	Out-of-phase	No-stimulation	One-way ANOVA	
				$F_{2,26}$	P
Sleep onset (min)	18.4 ± 3.4	13.6 ± 2.1	25.3 ± 5.4	$U_2 = 0.705$	0.703
Wake (min)	116.5 ± 9.4	126.7 ± 7.1	133.2 ± 5.6	0.156	0.857
NREM (min)	169.1 ± 11.3	189.1 ± 5.7	179.1 ± 5.4	$U_2 = 0.560$	0.756
REM (min)	23.2 ± 1.7	24.5 ± 0.9	24.5 ± 1.1	$U_2 = 4.319$	0.115

Mean (± SEM) sleep onset (duration to first transit into NREM sleep) and time spent in the different sleep stages during the 6-h retention interval. *F*- and *P*-values are indicated for one-way ANOVA across the three stimulation conditions. Non-parametric test (Kruskal-Wallis one-way ANOVA, U-statistics) were performed for failure to pass normality test (Kolmogorov-Smirnov). Note: There were no differences in sleep architecture between the stimulation conditions, which diverges from previous findings where much longer and more frequent stimulation enhanced NREM sleep (Kim et al, 2012).

Supplementary Table 2. Density of offline identified slow oscillations, spindles and ripple events. Related to Figure 1.

		In-Phase	Out-of-Phase	No-Stimulation	One-way ANOVA	
					$F_{2,26}$	P
Slow oscillations	FRO	37.82 ± 0.86	39.64 ± 0.52	37.88 ± 0.79	1.8404	0.185
	PAR	38.58 ± 0.87	39.76 ± 0.78	38.92 ± 0.69	0.580	0.567
Spindles	FRO	5.42 ± 0.13	5.33 ± 0.08	5.11 ± 0.10	2.567	0.096
	PAR	6.83 ± 0.22	6.96 ± 0.21	6.65 ± 0.23	0.513	0.605
	CA1	5.25 ± 0.35	5.11 ± 0.20	5.25 ± 0.35	0.058	0.944
Ripples	CA1	22.18 ± 1.50	19.56 ± 1.20	23.01 ± 1.26	3.397*	0.183

Mean (± SEM) density (per min) of offline detected slow oscillations (FRO and PAR), spindles (FRO, PAR and CA1) and hippocampal ripple events (CA1) during NREM sleep. *F*- and *P*-values are indicated for one-way ANOVA across the three stimulation conditions. FRO – prefrontal cortex and PAR – parietal cortex. * Kruskal-Wallis one-way ANOVA was used due to non-normal distribution of the data.

Supplementary Table 3. General characteristics of detected slow oscillations, spindles and ripple events (mean and SEM) for the 6-h recording period for the frontal (FRO), parietal (PAR) and hippocampal (CA1) electrode sites. Related to figure 4.

			In-phase	Out-of-phase	No-Stimulation	One-way ANOVA	
						$F_{2,26}$	*P*
Slow oscillations	FRO	Length (s)	0.582 ± 0.005	0.584 ± 0.006	0.583 ± 0.006	0.139	0.871
		Neg. Peak (mV)	-2.528 ± 0.153	-2.345 ± 0.188	-2.428 ± 0.179	0.251	0.780
		Amplitude (mV)	4.687 ± 0.284	4.336 ± 0.342	4.527 ± 0.324	0.278	0.760
	PAR	Length (s)	0.586 ± 0.007	0.606 ± 0.011	0.600 ± 0.007	3.031*	0.220
		Neg. Peak (mV)	-1.492 ± 0.084	-1.404 ± 0.118	-1.378 ± 0.085	0.385	0.684
		Amplitude (mV)	2.821 ± 0.162	2.587 ± 0.207	2.565 ± 0.148	0.670	0.520
Spindles	FRO	Length (s)	0.663 ± 0.002	0.654 ± 0.004	0.649 ± 0.004	4.366	**0.023**
		Frequency (Hz)	8.39 ± 0.01	8.38 ± 0.01	8.42 ± 0.02	1.268#	0.307
		Power (mV^2)	919.9 ± 48.1	759.0 ± 63.1	862.2 ± 40.6	2.456	0.105
	PAR	Length (s)	0.652 ± 0.003	0.652 ± 0.003	0.656 ± 0.006	0.414	0.665
		Frequency (Hz)	8.43 ± 0.01	8.41 ± 0.02	8.39 ± 0.02	1.054	0.363
		Power (mV^2)	688.8 ± 47.7	529.7 ± 58.6	543.6 ± 44.8	6.691*	**0.035**
	CA1	Length (s)	0.638 ± 0.003	0.642 ± 0.004	0.630 ± 0.005	$F_{2,22}$ = 2.038	0.154
		Frequency (Hz)	8.64 ± 0.01	8.64 ± 0.01	8.61 ± 0.01	$F_{2,22}$ = 3.474*	0.176
		Power (mV^2)	247.9 ± 44.6	158.2 ± 13.8	184.2 ± 27.7	$F_{2,22}$ = 2.123	0.144
Ripples CA1		Length (s)	0.054 ± 0.001	0.052 ± 0.001	0.054 ± 0.000	5.923*	0.052
		Frequency (Hz)	171.7 ± 1.5	168.1 ± 1.1	172.7 ± 1.6	$F_{2,22}$ =2.702	0.089
		Power (mV^2)	28.4 ± 4.5	36.9 ± 7.0	25.8 ± 4.3	$F_{2,22}$ =1.180	0.326

Data shown are mean ± SEM from the Prv-mhChR2-eYFP mice of the main fear conditioning experiment. * indicates Kruskal Wallis one-way ANOVA performed if non-normal distribution was confirmed. # indicates Welch robust test for equality of means following

failure to pass equality of variance test with normal distribution of the data. Significance is indicated by bold *P*-values.

Supplementary Table 4. Number of mice used for behavioral and electrophysiological recordings for the non-spindle-like (20Hz) stimulation experiment. Related to Figure 6.

			In-phase 20Hz
Prv-cre (FC)	DIO-YFP	Behavior	10 (10)
		EEG	10
	DIO-CHR2-YFP	Behavior	7 (7)
		EEG	7

Prv-cre mice were injected with AAV-EF1a-DIO-YFP or AAV-EF1a-DIO-ChR2-YFP (Channelrhodopsin2) and stimulated with an alternative stimulation (timing: in-phase, frequency: 20Hz, pulse duration: 5 ms; total duration of stimulation: 0.5s). Numbers of mice with both behavioral and electrophysiological recordings are indicated in brackets. EEG data are for both FRO and PAR leads.